Ocean Complexity Shapes Sea Surface Temperature Variability in a CESM2 Coupled Model Hierarchy

Sarah M. Larson,[a] Kay McMonigal,[a] Yuko Okumura,[b] Dillon Amaya,[d] Antonietta Capotondi,[c,d] Katinka Bellomo,[e,f] Isla R. Simpson,[g] and Amy C. Clement[h]

[a] *Department of Marine, Earth, and Atmospheric Sciences, North Carolina State University, Raleigh, North Carolina*
[b] *Institute for Geophysics, The University of Texas at Austin, Austin, Texas*
[c] *Cooperative Institute for Research in Environmental Sciences, University of Colorado Boulder, Boulder, Colorado*
[d] *NOAA/Physical Science Laboratory, Earth System Research Laboratory, Boulder, Colorado*
[e] *Department of Environment, Land and Infrastructure Engineering, Polytechnic University of Turin, Turin, Italy*
[f] *National Research Council, Institute of Atmospheric Sciences and Climate, Turin, Italy*
[g] *Climate and Global Dynamics Laboratory, National Center for Atmospheric Research, Boulder, Colorado*
[h] *Rosenstiel School of Marine and Atmospheric Science, University of Miami, Miami, Florida*

ABSTRACT: To improve understanding of ocean processes impacting monthly sea surface temperature (SST) variability, we analyze a Community Earth System Model, version 2, hierarchy in which models vary only in their degree of ocean complexity. The most realistic ocean is a dynamical ocean model, as part of a fully coupled model (FCM). The next most realistic ocean, from a mechanically decoupled model (MDM), is like the FCM but excludes anomalous wind stress–driven ocean variability. The simplest ocean is a slab ocean model (SOM). Inclusion of a buoyancy coupled dynamic ocean as in the MDM, which includes temperature advection and vertical mixing absent in the SOM, leads to dampening of SST variance everywhere and reduced persistence of SST anomalies in the high latitudes and equatorial Pacific compared to the SOM. Inclusion of anomalous wind stress–driven ocean dynamics as in the FCM leads to higher SST variance and longer persistence time scales in most regions compared to the MDM. The net role of the dynamic ocean, as an overall dampener or amplifier of anomalous SST variance and persistence, is regionally dependent. Notably, we find that efforts to reduce the complexity of the ocean models in the SOM and MDM configurations result in changes in the magnitude of the thermodynamic forcing of SST variability compared to the FCM. These changes, in part, stem from differences in the seasonally varying mixed layer depth and should be considered when attempting to quantify the relative contribution of certain ocean mechanisms to differences in SST variability between the models.

KEYWORDS: Atmosphere-ocean interaction; Oceanic mixed layer; Sea surface temperature; Climate models; Ocean models

1. Introduction

Identifying sources of climate variability, particularly as originating from the ocean or atmosphere, is a central scientific question with practical implications for predictability on time scales ranging from subseasonal to decadal and longer. The predictability of climate variations relies heavily on variability in the ocean, particularly from sea surface temperature (SST) anomalies. Compared to the atmosphere, the higher heat capacity of the ocean elongates the time scales of ocean thermal anomalies (Frankignoul and Hasselmann 1977; Bladé 1997; Barsugli and Battisti 1998), thereby supporting sustained SST anomalies that may in turn lead to a persistent ocean-forced atmospheric response (Bladé 1997). Seasonal variations in the mixed layer depth (MLD) can also trap wintertime thermal anomalies in the ocean's subsurface that then reemerge the following winter in the form of SST anomalies (Alexander and Deser 1995), leading to prediction skill at longer lead times in the North Pacific (Joh et al. 2022). In addition, the ocean dynamical response to the overlying winds often evolves on time scales longer than the wind variability itself, allowing ocean thermal variability to take on a lower frequency compared to the atmosphere, thus extending the potential predictability (Schneider et al. 2002). For example, anomalous wind stress curl on monthly time scales in the extratropical North Pacific can produce westward-propagating ocean Rossby waves that take years to cross the basin, generating decadal SST signals near the Kuroshio Extension region (Miller et al. 1998; Deser et al. 1999; Schneider and Miller 2001; Seager et al. 2001; Kwon and Deser 2007; Newman et al. 2016) and leading to longer lead prediction skill (Joh et al. 2022). On multiyear and decadal time scales, increased

---

McMonigal's current affiliation: College of Fisheries and Ocean Sciences, University of Alaska Fairbanks, Fairbanks, Alaska.

Corresponding author: Sarah M. Larson, slarson@ncsu.edu

Ocean and Coupled Air-Sea Processes	Model Version		
	FCM	MDM	SOM
Local ocean processes			
Vertical mixing and entrainment	✓	*B	
Seasonally varying mixed layer depth	✓	✓	
Multi-year persistence via the "reemergence" mechanism	✓	✓	
Ocean dynamical processes			
$\bar{v}\bar{T}$: Transport of the mean temperature by the mean ocean circulation	✓	✓	*P
$\bar{v}T'$: Transport of anomalous temperature by the mean ocean circulation	✓	✓	
$v'_{buoy}\bar{T}$: Transport of mean temperature by anomalous buoyancy-driven ocean circulation	✓	✓	
$v'_{\tau}\bar{T}$: Transport of mean temperature by anomalous wind stress driven ocean circulation	✓		
$v'_{buoy}T'$: Transport of anomalous temperature by anomalous buoyancy-driven ocean circulation	✓	✓	
$v'_{\tau}T'$: Transport by anomalous wind stress driven ocean circulation	✓		
Bjerknes feedback, as required for canonical ENSO	✓		
Thermodynamically coupled air-sea processes			
Atmospheric damping of SST	✓	✓	✓
Thermodynamic coupling	✓	✓	✓

FIG. 1. Ocean and coupled air–sea processes important for SST variability represented in the CESM2 SOM, MDM, and FCM. The term $P*$ indicates processes that are parameterized through the prescribed Q_{flx} in the SOM. The term $B*$ indicates that vertical mixing and entrainment related to anomalous wind stress–driven ocean circulation variability are absent. While the MDM includes many of the ocean and coupled air–sea processes simulated by the FCM, the MDM lacks any resulting variations that are driven by anomalous wind stress forcing on the ocean. The ocean circulation variability may include contributions from the AMOC in the FCM and MDM. See Larson et al. (2020) for further details.

predictability of upper ocean thermal variations in the North Atlantic (e.g., Smith et al. 2019) has been attributed to anomalous heat flux convergence in the subpolar gyre (Zhang et al. 2019; Yeager 2020).

Feedbacks between the atmosphere and the ocean also increase the persistence of SST anomalies (McCreary 1983; Latif and Barnett 1994; Gu and Philander 1997; Qiu 2003). For example, the atmosphere–ocean coupled Bjerknes feedback (Bjerknes 1969) in the tropical Pacific gradually amplifies SST anomalies, extending their lifetime and expanding their zonal extent throughout the tropical Pacific. Feedbacks between SST and clouds can enhance the variance of SST anomalies on decadal and longer time scales (Bellomo et al. 2014), as well as impact the frequency of El Niño–Southern Oscillation (ENSO) through coupling of the clouds to overlying circulation (Rädel et al. 2016; Middlemas et al. 2019). The cloud radiative effect (Hartmann and Short 1980; Norris and Leovy 1994) on SST also contributes to SST variability on climate time scales. Overall, slower ocean processes and coupled feedbacks can enhance the predictability of SST anomalies and the associated atmospheric circulation changes. Therefore, realistically representing these ocean-related processes in coupled climate simulations impacts the simulated spatial pattern, time scales, predictability, and impacts of SST variability.

On the one hand, improving the representation of ocean processes in coupled models is necessary to simulate the statistics of observed SST variability and coupling with the overlying atmosphere (e.g., Bellucci et al. 2021; Meccia et al. 2021; Putrasahan et al. 2021; Tsartsali et al. 2022). On the other hand, the complexity of the ocean and related processes complicates attribution studies. Indeed, many breakthroughs in climate dynamics have been made by stripping down complex coupled models into simpler forms. This approach has long been applied to uncover the physical processes necessary to explain midlatitude SST variability (Frankignoul and Hasselmann 1977; Frankignoul 1985; Barsugli and Battisti 1998; Alexander et al. 2000; Seager et al. 2000; Deser et al. 2003; Liu et al. 2023) and phenomenological SST variations like ENSO (e.g., Zebiak and Cane 1987; Suarez and Schopf 1988; Battisti and Hirst 1989; Jin 1997; Capotondi and Sardeshmukh 2015). These studies motivate the approach taken in this paper, to compare SST variability between a coupled model with a fully interactive dynamic ocean, hereafter referred to as a fully coupled model (FCM), and models with simpler representations of ocean processes.

An interactive dynamic ocean, as in FCMs, can alter SST through three broad categories of processes: 1) local ocean processes, 2) ocean dynamical processes, and 3) thermodynamically coupled air–sea processes (see Fig. 1, FCM column). We define local ocean processes as vertical ocean processes that can act to both damp and enhance SST anomalies, like mixing, entrainment, and processes that depend on the MLD like the reemergence mechanism (Alexander and Deser 1995). We define ocean dynamical processes as those that invoke either the seasonally varying climatological mean

$\overline{v}$ or anomalous v' ocean circulation to change SST through divergence of ocean heat transport vT, including features such as gyre circulations, overturning circulations, Ekman transports, and oceanic waves. The heat transport can be driven by wind stress (momentum) or by buoyancy fluxes, which consist of freshwater and thermal exchanges between the atmosphere and the ocean. The ocean heat transport can be decomposed into the following:

$$vT = \overline{v}\overline{T} + \overline{v}T' + (v'_{\text{buoy}}\overline{T} + v'_\tau\overline{T}) + (v'_{\text{buoy}}T' + v'_\tau T'), \quad (1)$$

which consists of the mean heat transport $\overline{v}\overline{T}$ (first term on the right-hand side), the anomalous transport of anomalous temperature T' by the mean circulation (second term), the anomalous transport of mean temperature by the anomalous circulation (third term), and the anomalous transport of anomalous temperature by the anomalous circulation (fourth term). The anomalous circulation is decomposed into that driven by anomalous wind stress v'_τ and anomalous buoyancy forcing v'_{buoy}. Dynamic ocean circulation variability is generally thought to enhance large-scale SST variability (Larson et al. 2018b), although with some exceptions related to Ekman transport in the subtropical oceans (Kang et al. 2008; Larson et al. 2018b; Small et al. 2020; Takahashi et al. 2021; Hasan et al. 2022). Dynamic ocean processes may also act to dampen SST variability, for example, through advection of mean ocean temperature. We stress that this decomposition is shown primarily to improve the conceptual understanding and distinction of processes between the hierarchy members. We acknowledge that this decomposition assumes that the buoyancy and wind stress contributions are roughly linear, which neglects the possible occurrence of nonlinear interactions between the different processes.

We define thermodynamically coupled air–sea processes as those in which the SST is thermodynamically coupled to changes in the atmosphere, including the damping of SST anomalies through turbulent heat fluxes (e.g., Newtonian cooling) and the generation of SST anomalies through processes such as the wind–evaporation–SST (WES; Xie and Philander 1994) and cloud–SST feedbacks. Specifically, these are local thermodynamically coupled processes where air–sea heat exchange leads to the anomalous SST without invoking ocean circulation changes. Hereafter, "ocean damping" refers to all ocean processes that may damp SST anomalies, including vertical mixing, entrainment, mixed layer depth processes, and advection by the mean ocean circulation.

Evaluating the role of a dynamic ocean on SST variability is often done through comparisons between a FCM and a version of the model in which the dynamic ocean is replaced with a thermodynamic mixed layer, often referred to as a slab ocean model (SOM; see the SOM column in Fig. 1 for related processes). The thermodynamic mixed layer ocean allows for consistency between the air–sea heat fluxes and changes in the underlying ocean temperature and modifies the representation of the atmospheric circulation and heat flux response to SST (Saravanan and Chang 1999; Yulaeva et al. 2001; Sutton and Mathieu 2002). SST variations that occur only in the FCM or SST anomaly patterns that have significantly different

variances when comparing the SOM with the FCM indicate a role for interactive ocean dynamics (Gozdz et al. 2024). Indeed, SOMs can simulate unrealistically high SST variability, presumably due to the lack of ocean damping (Murphy et al. 2021; Liu et al. 2023). Often it is assumed that if similar climate variations occur in the SOM and FCM versions, ocean dynamics are considered unnecessary to generate the variability. However, this argument is sometimes difficult to support, as SOMs lack both ocean processes that damp SST anomalies as well as ocean dynamics known to amplify SST variance. Therefore, if similar magnitude SST variability occurs in the SOM as the FCM, it may be for different physical reasons, although this can be difficult to prove (Clement et al. 2015; Zhang et al. 2016; Cane et al. 2017). Another complicating factor is that SOMs generally apply a time-invariant MLD which impacts MLD processes important for SST variability (Bitz et al. 2012; Yamamoto et al. 2020; Liu et al. 2023). Overall, these disparities make it difficult to attribute differences or similarities in the SOM and FCM SST to specific oceanic or coupled air–sea processes.

The present study addresses the above concerns by analyzing monthly SST variability in a coupled model hierarchy with an intermediate step between SOM and FCM versions, allowing for attribution of the different ocean and air–sea coupled processes associated with an interactive ocean in driving SST. This intermediate step is a mechanically decoupled model (MDM; Larson and Kirtman 2015; Larson et al. 2017, 2018b, 2020). The MDM includes the same dynamic ocean model as the FCM, but the ocean lacks anomalous wind stress–driven ocean dynamics (Fig. 1, MDM column). Therefore, SST variations in the MDM are buoyancy forced, which includes contributions from air–sea thermodynamics as well as ocean dynamics driven by buoyancy forcing, whereas variations in the SOM are strictly forced by air–sea thermodynamics. However, the presence of the seasonally varying ocean circulation and MLD, as well as anomalous buoyancy-forced ocean dynamics like the basin-scale Atlantic meridional overturning circulation (AMOC), can also modify SST variability in the MDM. Importantly, key sources of ocean damping are also present in the MDM, including vertical mixing, entrainment, and advection by the mean ocean circulation, whereas many dynamical sources of SST variability, as facilitated through anomalous wind stress–driven ocean dynamics, are absent. More generally, the MDM contains more ocean processes than the SOM, but fewer than the FCM. Comparing the SOM and MDM can uncover the collective role of MLD variability, buoyancy coupled ocean dynamics, and ocean damping on climate variations, whereas comparing the MDM and FCM can uncover the role of wind stress–driven ocean dynamics on SST variability. We present considerations for interpreting the relative contribution of these different physical processes in this paper.

While previous studies have compared SST variations between SOM and FCM simulations (e.g., Bitz et al. 2012; Clement et al. 2011, 2015; Murphy et al. 2021) and MDM versus FCM simulations (Larson et al. 2017, 2018b; Zhang et al. 2021; Luongo et al. 2024), to our knowledge, this is the first attempt to systematically analyze all three versions together to diagnose the role of ocean processes and MLD climatologies
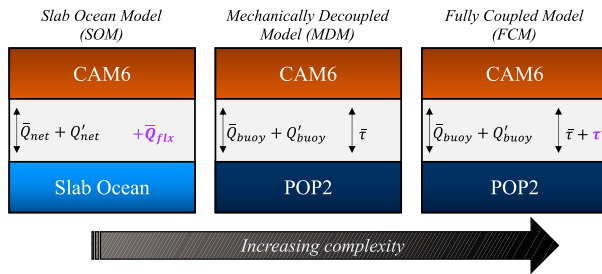
FIG. 2. Summary of the CESM2 hierarchy. POP2 refers to the dynamic ocean model in CESM2. CAM6 refers to the atmosphere model. In the SOM, $\overline{Q}_{\text{net}}$ is the monthly climatology of the net air–sea heat flux. The term Q'_{net} is the anomalous air–sea heat flux, and $\overline{Q}_{\text{flx}}$ represents the prescribed monthly climatology of ocean heat transport convergence described in section 2c. In the FCM, the climatological buoyancy fluxes $\overline{Q}_{\text{buoy}}$ and wind stress forcing on the ocean $\overline{\tau}$ and the related anomalies Q'_{buoy} and τ' drive the mean and anomalous ocean circulation. The MDM is similar to the FCM, except that τ' cannot drive changes in the ocean circulation.

in driving anomalous SST. The paper is organized as follows. Section 2 introduces the Community Earth System Model, version 2 (CESM2), hierarchy and observational datasets. Section 3 introduces analysis methods. Section 4 compares the MLD climatology, annual-mean SST, and SST variability between the model versions and investigates the role of ocean processes and MLD differences to understand the SST differences. Sections 5–7 include a summary, implications, and discussion, respectively.

2. CESM2 hierarchy

All model versions analyzed in this study originate from the CESM2 (Danabasoglu et al. 2020) base code. Figure 2 shows a schematic representation of the air–sea coupling and ocean component of each hierarchy member considered in this study. Hierarchy members are introduced in order from most to least ocean complexity, beginning with the FCM.

a. FCM

CESM2 is a state-of-the-art fully coupled model consisting of atmosphere, ocean, land, and sea ice, and while it has the capability of simulating the Greenland ice sheet, the simulations here assume fixed ice sheets (Danabasoglu et al. 2020). The individual interactive model components are the Community Atmosphere Model, version 6 (CAM6), the Parallel Ocean Program, version 2 (POP2; Smith et al. 2010), the Community Land Model, version 5 (CLM5; Lawrence et al. 2019), and the Los Alamos Community Ice Code, version 5 (CICE5; Hunke et al. 2015), sea ice model. The model components exchange fluxes through the Common Infrastructure for Modeling the Earth (CIME) coupler framework. The CAM6 and POP2 model simulate the general circulation of the atmosphere and ocean, respectively.

All configurations of CESM2 considered in this comparison are of nominal 1° horizontal resolution. In CAM6 and CLM5, the latitudinal grid spacing is 0.9°, longitudinal grid spacing is 1.25°, and the vertical dimension of CAM6 is divided into 32

levels with a model top at around 40 km. Both POP2 and CICE5 have a variable latitudinal grid with finer resolution at the equator of 0.27°, uniform longitudinal grid of 1.125°, and 60 vertical levels. The vertical levels are uniformly distributed every 10 m in the upper 160 m and gradually coarsen in depth below. All configurations are run with fixed preindustrial radiative forcing from the year 1850, so climate variations in all models are due to natural variability and not changes in external forcing. The FCM analyzed in this study is the version of CESM2 that contributed to phase 6 of Coupled Model Intercomparison Project (CMIP6; Eyring et al. 2016) and is freely available on NCAR's Climate Data Gateway. We analyze model years 1100–1699, a total of 600 years. These model years match those from the MDM (section 2b) and allow for spinup of the deep ocean.

In the FCM, the ocean is coupled to the atmosphere through buoyancy and momentum fluxes (Fig. 2, FCM panel). Momentum fluxes represent the stress imparted on the ocean via wind stress τ. The τ can be decomposed into climatological $\overline{\tau}$ and anomalous τ' components. Buoyancy fluxes Q_{buoy} are defined as the sum of the net air–sea heat fluxes Q_{net} and freshwater fluxes Q_{fw}. The Q_{net} consists of incoming shortwave and outgoing longwave radiative heat fluxes and sensible and latent heat fluxes. Climatological buoyancy fluxes are represented by $\overline{Q}_{\text{buoy}}$. Ocean variability is typically generated through anomalous exchanges of buoyancy Q'_{buoy} and anomalous momentum τ' fluxes. We refer to the contribution of the latter term as τ' dynamics or anomalous wind stress–driven ocean dynamics. The coupling frequency of the ocean model is hourly; therefore, each forcing term is computed in CIME for each model hour.

b. MDM

To determine the relative role of τ' dynamics on SST, we integrate a mechanically decoupled version (Larson and Kirtman 2015; Larson et al. 2017, 2018b, 2020; McMonigal et al. 2023) of CESM2 to compare with the FCM. In the MDM, the ocean circulation is driven by the seasonal cycle of $\overline{\tau}$ along with $\overline{Q}_{\text{buoy}}$ and Q'_{buoy}. However, τ' and the related τ' dynamics cannot drive changes in ocean circulation (see Fig. 1, MDM column; Fig. 2, MDM panel), leaving ocean circulation variability generated solely through anomalous buoyancy fluxes Q'_{buoy}. SST variations may also be generated through the advection of SST anomalies by the mean ocean circulation. Hence, we refer to this ocean representation as a buoyancy coupled dynamic ocean. If SST variations are present and have similar variance in both the MDM and the FCM, then they are considered buoyancy forced.

The MDM version is implemented by overwriting the τ forcing on the ocean with climatological wind stresses $\overline{\tau}$ computed from the FCM. The temporal resolution of $\overline{\tau}$ is 6-hourly to resolve the seasonal and diurnal cycles. To obtain the FCM's 6-hourly zonal and meridional τ component climatologies, we rerun the FCM for 50 years from the model restart files originating from the year 1051, output hourly τ from CIME, and compute the 6-hourly climatologies over the 50-yr period. A 6-hourly climatology is chosen to reduce the local memory required for the forcing files while retaining the

diurnal cycle. Using CIME output ensures the climatologies are in the identical format POP2 expects and no remapping onto the POP2 grid is necessary, thereby eliminating potential interpolation errors. Given that CIME communicates information, including τ, to the ocean once every hour, we use the first 6-hourly climatology on a given day to force the ocean from 0001 to 0600 LT, the second 6-hourly climatology for daily hours 0601–1200 LT, and so on. Prescribing the $\overline{\tau}$ from the FCM is critical to obtain a cleaner comparison to the FCM, as prescribing climatology from reanalysis products can severely modify the tropical Pacific mean state (Larson et al. 2017). Notably, wind variability is still included in the bulk formula for turbulent heat fluxes; thus, the MDM remains thermodynamically coupled (e.g., Ding et al. 2014, 2015). Note that to maintain comparable mean state sea ice between the FCM and the MDM, decoupling is not applied to the atmosphere-to-sea ice stress. When mechanical decoupling is applied to the atmosphere-to-sea ice stress, the sea ice adjusts to its thermodynamic equilibrium, resulting in a vastly different sea ice mean state compared to the FCM. The MDM is branched from the FCM restart files from model year 1051. Years 1100–1699, a total of 600 simulation years, are analyzed here. This simulation is also freely available on NCAR's Climate Data Gateway.

c. SOM

The simplest ocean representation analyzed in this study is the SOM version of CESM2 (Fig. 2). In this configuration, CAM6 is coupled to a motionless mixed layer ocean model (see Bitz et al. 2012). Similar to the FCM and MDM, the SOM includes a dynamic sea ice model CICE5. As typically done with SOMs, to simplify the mixed layer temperature tendency equation, the MLD in the SOM is prescribed as the annual-mean MLD from the FCM, which varies spatially.

To closely reproduce the SST mean state and seasonal cycle from the FCM, the SOM includes a $\overline{Q}_{\mathrm{flx}}$ term (Fig. 2, SOM panel) in the mixed layer temperature tendency equation that attempts to represent the monthly climatological ocean heat transports that are present in the FCM. A time-varying Q_{flx} is first calculated from 50 years of a FCM CESM2 simulation as follows:

$$Q_{\mathrm{flx}} = \rho_0 c_p \overline{H} \frac{dT_{\mathrm{mix}}}{dt} - Q_{\mathrm{net}}, \qquad (2)$$

where ρ_0 is the density of seawater, c_p is the heat capacity of seawater, $\overline{H}$ is the annual-mean MLD, dT_{mix}/dt is the mixed layer ocean temperature tendency, and Q_{net} is the net air–sea heat flux from the ocean model. The $\overline{Q}_{\mathrm{flx}}$ term is then computed monthly to obtain a monthly varying climatology of the FCM ocean transport effects. See He et al. (2022) for caveats to this approach if Q_{net} is obtained from the atmosphere instead of ocean output. This $\overline{Q}_{\mathrm{flx}}$ term is added to the energy balance equation in the SOM. Finally, the global energy imbalance is subtracted to maintain a net zero global flux. Despite this careful approach, differences between the SOM and the FCM do emerge in the mean and seasonal cycle, particularly in the subpolar North Atlantic, where differences approach 1°C. The difference in the globally averaged annual-mean SST between the SOM and the FCM is 0.26°C, closely

matching the 0.3°C difference found between the CCSM4 SOM and FCM (Bitz et al. 2012). These differences are discussed further in section 4b.

Note that the 50-yr FCM simulation used to estimate $\overline{H}$ and $\overline{Q}_{\mathrm{flx}}$ in the SOM, hereafter referred to as FCM$_{50}$, is a different version of the CESM2 FCM than that analyzed in this study. In the FCM$_{50}$, the sea ice albedos were altered to generate more realistic ice in the central Arctic compared to the previous version of the SOM with too thin sea ice. However, FCM$_{50}$ has a similar annual-mean SST to the FCM (not shown); therefore, differences in the mean SST from the SOM compared to the other hierarchy members appear unrelated to deriving $\overline{H}$ and $\overline{Q}_{\mathrm{flx}}$ from a slightly different FCM version. A total of 360 years of the SOM are analyzed, and the last 350 years are used in the analysis to avoid spinup issues.

3. Analysis methods

The objective of this analysis is to compare SST variability across the CESM2 hierarchy. For the MDM and the FCM, SST is defined as the uppermost level of the ocean temperature variable TEMP. For the SOM, SST is defined from the surface temperature TS variable, excluding grid points that have any fraction of sea ice or land or where TS is missing for over half the time period due to seasonality in sea ice coverage. The former is to eliminate grid points where TS deviates from SST, as TS represents the weighted average of surface temperature over different surface types. The latter is to eliminate grid points where TS will be biased toward the summer season. For comparison with the CESM2, observed SST is taken from the NOAA Extended Reconstructed SST version 5 (ERSST.v5; Huang et al. 2017) over 1950–2020. ERSST.v5 is on a 2° × 2° horizontal grid.

The SST variability is estimated by computing the monthly anomaly variance. Monthly anomalies are calculated by removing the monthly climatology from the respective model. Variances between model pairs are compared by calculating the common (i.e., base 10) logarithm of the SST variance ratio for each model pair at each grid point:

$$X = \log_{10}\left(\frac{\sigma_c^2}{\sigma_s^2}\right), \qquad (3)$$

where σ_c^2 and σ_s^2 represent the variances from the hierarchy member with the more complex and simpler ocean models, respectively.

The persistence of SST anomalies is estimated using a decorrelation measure proposed by DelSole (2001). The persistence time scale, or T_2 as in DelSole (2001) and Buckley et al. (2019), is calculated as

$$T_2 = 1 + 2\sum_{k=1}^{\infty} \rho_k^2, \qquad (4)$$

where ρ_k is the autocorrelation of anomalous SST at lag k months. This approach is ideal for persistent anomalies that may also be oscillatory.
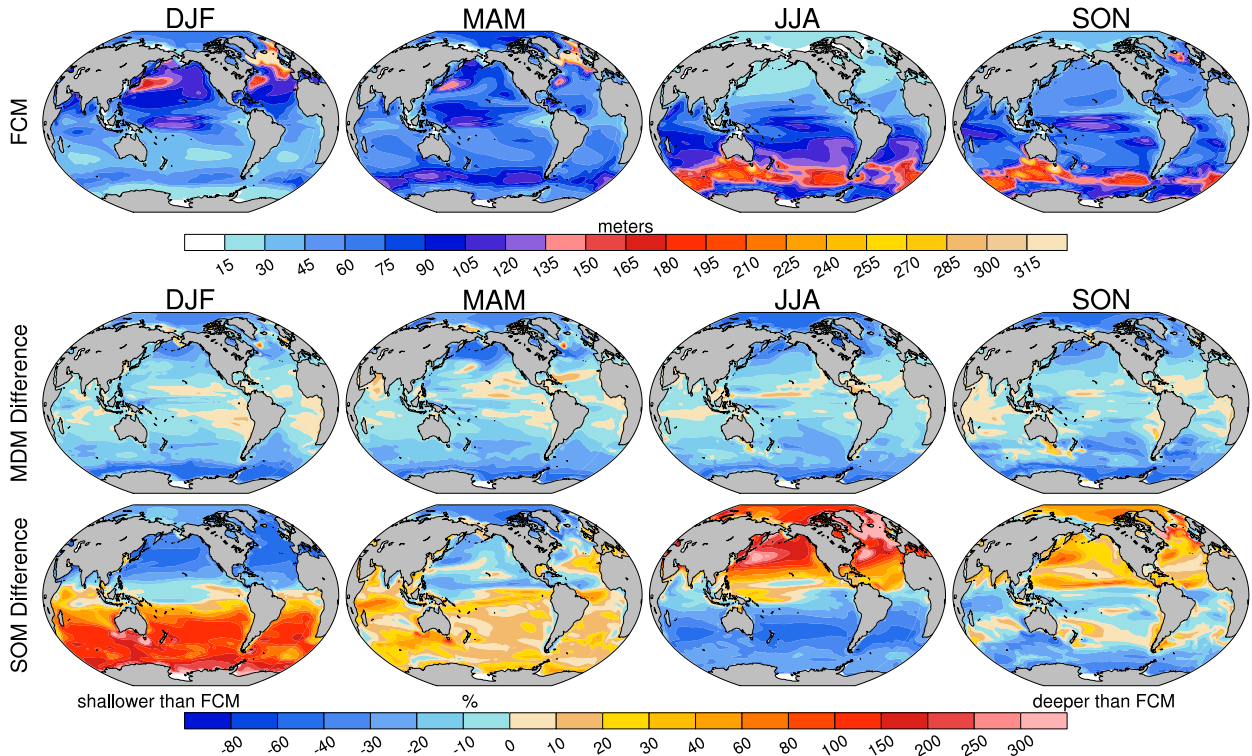
FIG. 3. (top) Climatological seasonal MLD (m) from the FCM. (middle) Percent difference in the seasonal mean MLD in the MDM compared to the FCM, normalized by the FCM, calculated as $100 \times$ (MDM − FCM)/FCM. (bottom) Percent difference in the seasonal mean MLD in the SOM compared to the FCM, normalized by the FCM. Positive values indicate that the MLD in the less complex model (SOM or MDM) is deeper than that in the FCM. The MLD is obtained from the POP2 output variable HMXL, which is roughly estimated as the depth of the maximum buoyancy gradient.

Following Alexander and Penland (1996) but ignoring effects due to entrainment into the mixed layer, we estimate the anomalous SST tendency driven by air–sea heat fluxes as

$$\frac{\partial \text{SST}'}{\partial t} \approx \left(\frac{Q_{\text{net}}}{\rho_0 c_p H} \right)', \quad (5)$$

$$\left(\frac{Q_{\text{net}}}{\rho_0 c_p H} \right)' \approx \frac{Q'_{\text{net}}}{\rho_0 c_p \overline{H}} - \frac{\overline{Q}_{\text{net}} H'}{\rho_0 c_p \overline{H}^2} - \left(\frac{Q'_{\text{net}} H'}{\rho_0 c_p \overline{H}^2} - \frac{\overline{Q'_{\text{net}} H'}}{\rho_0 c_p \overline{H}^2} \right), \quad (6)$$

where H is the MLD, Q_{net} is the net heat flux from the ocean model oriented positively downward, ρ_0 is the density of seawater, and c_p is the heat capacity of seawater. The overbar indicates the monthly mean climatology, and the prime indicates the monthly anomaly. We refer to the first, second, and third (in parentheses) terms on the right-hand side of Eq. (6) as the Q', H', and $Q'H'$ terms, respectively, and the term on the left-hand side as the Q'_{total} term. The H' term represents variations due to anomalies in the MLD, whereas $Q'H'$ is the contribution related to the covariance of MLD and heat flux anomalies. The latter tends to be largest in regions of deep convection where MLD variations are strongly tied to Q', and this contribution could be underestimated by using monthly data. Through a Taylor series expansion, Alexander and Penland (1996) use the approximation $H'/\overline{H} \ll 1$ to obtain

the right-hand side of Eq. (6). While their approximation is based on daily MLD, we find that this assumption generally holds for the seasonal time scales (e.g., DJF, MAM, JJA, and SON) although the ratio approaches 1 in areas of deep convection in the North Atlantic during DJF and MAM (not shown). In the SOM, $\overline{H}$ is set as the spatially varying annual-mean MLD from the FCM or $\overline{H}(x, y)$; thus, the denominator on the left-hand side of Eq. (6) for the SOM is constant and this term is equivalent to the Q' term. We compute and compare the variances of each term on the right-hand side of Eq. (6), as applicable, across the simulations.

Finally, as our intent is to investigate how different $\overline{H}$ and resolved ocean processes may influence SST variability in the simulations considered, we recompute each term on the right-hand side of Eq. (6) for each simulation but using the monthly MLD climatology from the FCM for all models. This way, if the variances of the individual terms from the MDM and the SOM become more comparable to that from the FCM when computed using the FCM MLD, we can hypothesize that differences in $\overline{H}$ contribute to the SST variance differences.

4. Results

a. Climatological mixed layer depth

The climatological MLD in the FCM varies seasonally and is deeper in the winter hemisphere and shallower in the summer
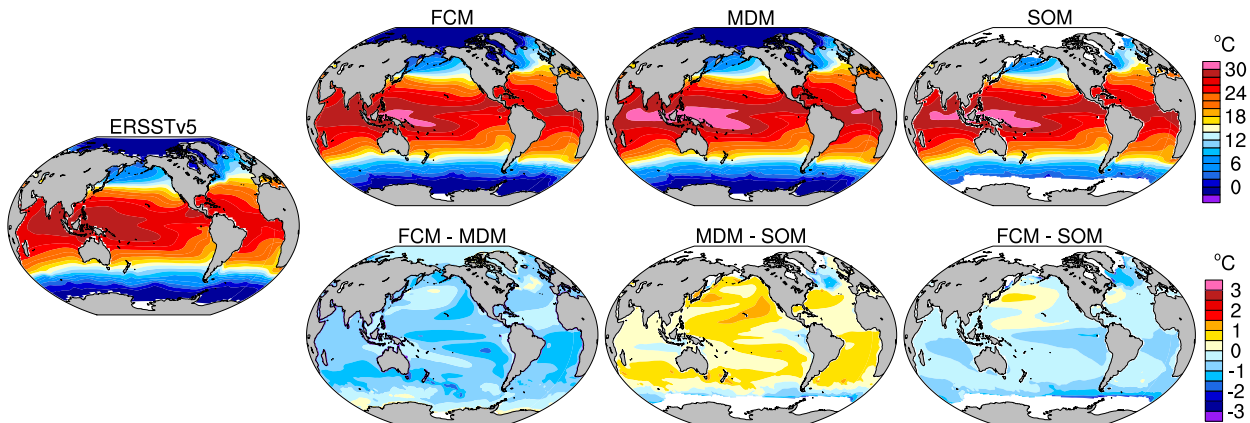
FIG. 4. Annual-mean SST (°C) from observations (ERSST.v5), the model hierarchy members, and the differences between each model pair. In the difference plots, positive values indicate the model version with more complex ocean processes is relatively warmer.

hemisphere (Fig. 3, top row). Given that the SOM has a seasonally invariant MLD, the climatological MLD in the SOM is overestimated in the summer hemisphere and underestimated in the winter hemisphere compared to the FCM (Fig. 3, bottom row). In fact, during JJA, the MLD in the SOM is over 300% deeper than that in the FCM in the Kuroshio–Oyashio Extension (KOE) and Gulf Stream Extension regions as well as most of the high-latitude North Atlantic. In DJF, the Southern Hemisphere too shows an overestimated MLD in the SOM, but to a lesser degree.

The seasonally varying climatological MLD in the MDM is shallower than that in the FCM in nearly all regions, as seen in prior MDM versions of CESM (e.g., Larson et al. 2018b) and as reported in McMonigal et al. (2023) for CESM2. The shallower MLD in the MDM is due to the lack of τ' dynamics on submonthly time scales, which act to deepen the MLD in the FCM through mixing and entrainment of colder deeper waters into the mixed layer (see Luongo et al. 2024). The difference in the MLD is most pronounced in the extratropics where wind variability is typically largest. The MLD differences between the MDM and the FCM do not change appreciably between seasons and are notably smaller than the differences between the SOM and the FCM, especially in the winter and summer hemispheres. We expect the large seasonal differences in the MLD between the SOM and the FCM and the year-round shallower MLD in the MDM compared to the FCM to impact the overall SST variability, particularly through contributions to SST changes as in Eq. (6).

b. Annual-mean SST

We next compare the annual-mean SST across models. The FCM reproduces the general features of the annual-mean SST from observations (Fig. 4) but is slightly warmer in the global mean than ERSST.v5 (Danabasoglu et al. 2020). The FCM is cooler than the MDM nearly everywhere, as indicated by the negative values in the FCM minus MDM difference plot. Overall, compared to the MDM, the cooler SST and deeper MLD in the FCM are evidence of the rectification of τ'-driven variability onto the mean SST. The lack of this effect in the MDM can manifest in two ways that may result in

relatively warmer annual-mean SST compared to the FCM: 1) The MDM lacks τ' dynamics that may act to cool the mean SST through wind stress–driven deepening of the MLD and the associated entrainment of cold water from below and 2) the shallower MLD in the MDM then results in the distribution of $\overline{Q}_{net}$ over a shallower depth, further warming the mean SST compared to the FCM. Following Sutton et al. (2024), differences in the extratropical SST mean state could, in part, be related to the asymmetry of extratropical teleconnections due to ENSO via the "atmospheric bridge" mechanism (Lau and Nath 1996). Surprisingly, the SST difference pattern in the CESM2 versions of the FCM and MDM differs from that in predecessor versions, namely, CESM1-CAM4 (not shown) and CESM1 (Luongo et al. 2024). We hypothesize that the ubiquitously warmer SST in the CESM2 MDM compared to the FCM could also be related to the more positive low cloud–SST feedback in CESM2 compared to the predecessor versions (e.g., Kim et al. 2022 and Fig. S1 in the online supplemental material). The more positive cloud feedback in CESM2 could act to warm the overall SST, whereas the same feedback is weak in CESM1 versions.

The MDM is warmer than the SOM nearly everywhere, which can be linked to the fact that the MLD in the SOM is set to the annual-mean MLD from the FCM. The annual-mean MLD in the MDM is shallower than the MLD in the SOM, thus distributing $\overline{Q}_{net}$ over a shallower depth. The more efficient heating of the mixed layer and possible amplification of the heating due to the strong low cloud–SST feedback then could result in a relative warming in the MDM.

The FCM annual-mean SST is cooler than the SOM SST everywhere except near the Northern Hemisphere western boundary current extensions. There are, however, seasonal SST differences between the SOM and the FCM that suggest that the annual-mean differences are, in part, related to differences in the seasonal MLD between the models. For example, in boreal summer, the FCM SST is warmer than the SOM throughout much of the Northern Hemisphere (Fig. S2, JJA) when the FCM MLD is substantially shallower than that in the SOM (Fig. 3, bottom row). The shallower MLD in the FCM allows for more efficient daytime heating of the mixed
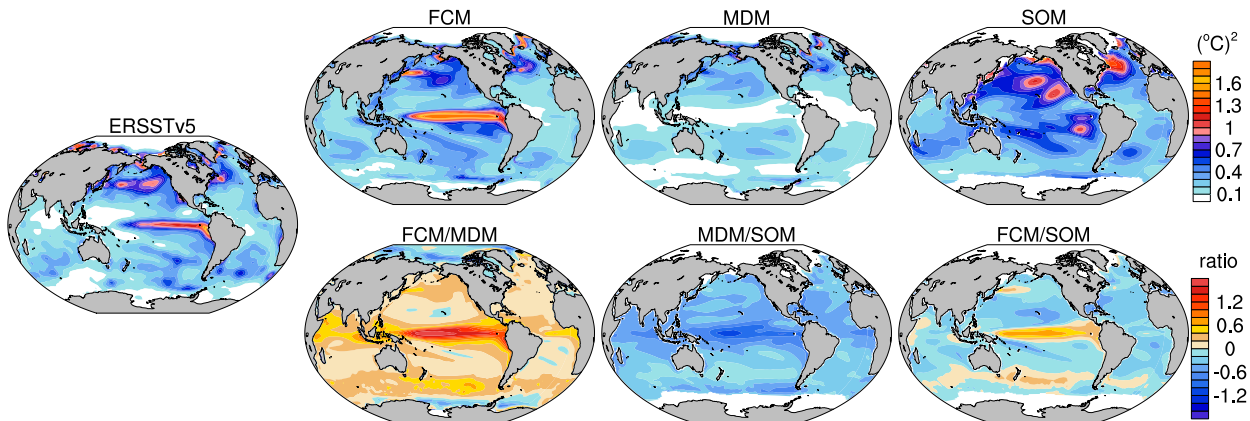
FIG. 5. Monthly SST variance $(°C)^2$ from observations (ERSST.v5) and the CESM2 hierarchy members. The bottom-right three panels show the common logarithm ratio of SST variance between each model pair. Positive values indicate the model version with the more complex ocean, indicated in the numerator, has higher SST variance at a particular grid point. Negative values indicate the model with the simpler ocean, indicated in the denominator, has more SST variance. A log-ratio value equal to 1 indicates the model with the more complex ocean has 10 times (i.e., 10^1) higher variance, whereas a log-ratio value of −1 indicates the model with the simpler ocean has 10 times higher variance.

layer, resulting in relatively warmer SST compared to the SOM. Similarly, when the FCM MLD is shallower than that in the SOM during austral summer (DJF), the FCM shows regions of relatively warmer SST than the SOM in the subtropical Southern Hemisphere. In the winter hemisphere, the SOM MLD is shallower than that in the FCM which we expect would strengthen wintertime cooling, but instead the SOM SST is warmer than the FCM. The SOM is also overall warmer than the FCM in CCSM4 (Bitz et al. 2012). It is possible that the warmer SOM SST is related to the experimental design of the SOM. In the SOM, the global energy imbalance is subtracted at all grid points to maintain a net zero global flux [see Eq. (2)], thereby potentially creating sources and sinks of energy in the SOM. This could manifest as a net warming in many regions in the SOM, resulting in the FCM being relatively cooler than the SOM. This same effect would also manifest in the MDM and SOM comparison, except that the MDM lacks the rectification of τ' dynamics onto the mean state that results in a relative cooling in the FCM. Without this cooling effect, the MDM could remain warmer than the SOM, explaining the differences between the two models. Differences in the annual-mean SST between the SOM and the FCM could also be, in part, linked to rectified effects of nonlinearities such as amplitude asymmetry related to ENSO present in the FCM but not in the SOM.

However, we would expect that for ENSO amplitude asymmetry, that El Niño events tend to be stronger than La Niña events, the FCM mean tropical SST would be more El Niño–like compared to the SOM, but that is not the case.

c. Anomalous SST variance

The FCM reproduces the general spatial pattern of monthly SST variance from observations with a few notable exceptions (Fig. 5). Capotondi et al. (2020) show that CESM2 exhibits higher-amplitude ENSO variability than observations, and this overestimation in the equatorial eastern Pacific is reflected in the higher SST variance seen in the FCM versus the ERSST.v5. The FCM also exhibits higher SST variance near the Kuroshio Extension but lower variance in the Gulf Stream Extension and central North Pacific compared to observations.

The SOM shows distinct centers of relatively higher SST variance in the North Atlantic, northeast and southeast subtropical Pacific, and central North Pacific. These centers of relatively large SST variability coincide with regions of climatologically high wind variability that can drive SST variations through modulating the turbulent heat fluxes. However, differences in low-level wind variability between the models cannot explain the differences in SST variability in these regions,
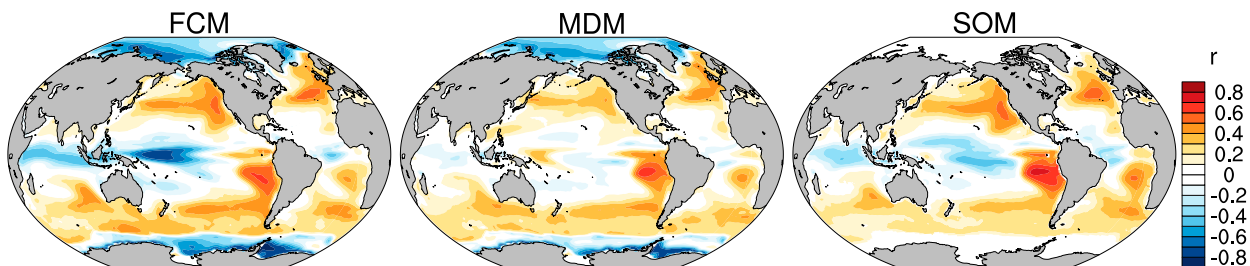

FIG. 6. Correlation between monthly SST and downward SWCF anomalies for each CESM2 version.

as the models simulate similar magnitudes of 10-m wind speed variance away from the tropics (Fig. S3). Instead, with the exception of parts of the North Atlantic, these regions approximately coincide with where the shortwave cloud forcing (SWCF) and SST correlation are positive in CESM2 (Fig. 6), indicating positive feedback between the SWCF and the SST. The MDM shows relatively high SST variance in these same regions, but the amplitude of the variance is substantially lower when compared to the SOM. We hypothesize that due to the lack of ocean damping in the SOM, cloud feedbacks and turbulent heat flux anomalies make a stronger imprint on SST variability than in the MDM.

Following Murphy et al. (2021), in Fig. 5 we compare the SST variability between the models by computing the common logarithm of the SST variance ratio for each model pair [Eq. (3)]. Compared to the FCM, the MDM exhibits noticeably lower SST variance nearly everywhere, as indicated by the predominantly positive FCM/MDM log-ratio values. These results indicate that τ' dynamics generally enhance SST variability globally, consistent with an earlier version of the MDM (Larson et al. 2018b). The reduced variability in the MDM could be, in part, due to the lack of ENSO teleconnections, particularly in regions like the North Pacific and tropical ocean basins. Due to the lack of ENSO in the MDM (e.g., Fig. S4), the FCM exhibits over 10 times the amount of SST variance in the tropical Pacific compared to the MDM. The FCM also produces higher SST variance in the KOE region, as expected given that τ' dynamics play a key role in generating interannual and decadal SST variability in the western North Pacific (Miller et al. 1998; Deser et al. 1999; Ferreira et al. 2001; Schneider and Miller 2001; Seager et al. 2001; Qiu 2003; Kwon and Deser 2007). Similarly, τ' dynamics, particularly anomalous wind stress–driven Ekman advection, have been shown to drive SST variability throughout the Southern Ocean where zonal wind variability efficiently drives temperature advection across the mean meridional SST gradient (Rintoul and England 2002; Dong et al. 2007). In the tropical Indian Ocean, the Indian Ocean dipole SST pattern, which is driven by τ' dynamics both related and unrelated to ENSO (Yang et al. 2015; Stuecker et al. 2017; McMonigal and Larson 2022), contributes to the larger variance in the FCM. In the tropical Atlantic Ocean, τ' dynamics drive SST variability associated with the Atlantic Niño (Zebiak 1993; Lübbecke et al. 2018), thus resulting in larger variance in the FCM compared to the MDM. We note that all models considered include an active WES feedback; therefore, the general SST characteristics associated with thermodynamically coupled meridional modes (e.g., see Amaya 2019 review) have been identified in each of these model types (Zhang et al. 2014; Larson et al. 2018a; Zhang et al. 2021).

One notable exception in the FCM and MDM comparison is the slightly higher SST variance in the Pacific subtropics in the MDM compared to the FCM. Anomalous wind stress–driven Ekman advection damps thermodynamically driven SST variability throughout the subtropics (Larson et al. 2018b; Hasan et al. 2022), resulting in relatively higher SST variance in the MDM, where the effect is absent. The Ekman advection damping of the SST variance is more pronounced

in a predecessor version of CESM2 (Larson et al. 2018b). We hypothesize this model dependence could be related to differences in the shortwave cloud–SST feedback, which is substantially stronger in CESM2 than its predecessor versions (Kim et al. 2022) and could impact the strength of the WES feedback, but this requires further investigation.

The SOM generally has higher SST variance than the FCM, indicated by negative log-ratio values in the FCM and SOM comparison (Fig. 5), except in the equatorial Pacific, KOE region, and the Southern Ocean. In these three regions, τ' dynamics drive SST variability in the FCM that is absent in the SOM (and MDM). Elsewhere, damping due to the dynamic ocean in the FCM appears to dominate the differences in the SST variance between the FCM and the SOM. Moreover, the SOM has higher SST variance than the MDM everywhere, indicating that without τ' dynamics, the ocean plays a net damping role to thermodynamically driven SST variability. In the MDM and SOM, SST variability is primarily thermodynamically driven, but in the MDM, the SST variability can be damped by the mean ocean advection, vertical entrainment, and mixing.

For each comparison between model pairs, the sign of the log-ratio values and the overall patterns are generally consistent across seasons (see Figs. S5–S8) suggesting that differences in ocean processes simulated are playing an important role in the variance differences. For example, the SST variance is larger in the SOM than in the MDM even during seasons when the MLD in the MDM is substantially shallower (e.g., the summer hemisphere), which we expect would primarily enhance thermodynamically driven SST variability. However, the MDM SST variance remains lower than that in the SOM across all seasons, indicating that processes in the ocean that damp SST anomalies are an important contributor to the differences, as shown in Liu et al. (2023) for the North Atlantic. The variance in the FCM is larger than in the MDM during all seasons, except in the small regions of the subtropics due to Ekman damping, indicating that τ' dynamics are a primary contributor to the differences. The fact that these differences persist across seasons, particularly for the SOM, indicates that seasonally varying differences in the MLD are not the only contributor to the overall variance differences. Section 4e will further investigate the impact of the different climatological MLDs.

d. Anomalous SST persistence

Inclusion of a buoyancy coupled dynamic ocean as in the MDM leads not only to dampening of SST variance everywhere (Fig. 5) but also reduced persistence of SST anomalies in the high latitudes and equatorial Pacific (Fig. 7) compared to the SOM. The persistence of SST anomalies in parts of the Southern Ocean in the SOM is roughly 1 year longer than that in the MDM (and the FCM). SST anomalies persist for 4–8 months longer in the SOM than the MDM (and the FCM) in the North Pacific. SST anomalies in the SOM have longer persistence than the FCM in similar regions, including the Southern Ocean, parts of the North Atlantic, KOE, tropical Pacific, and the Gulf Stream Extension, indicating that the
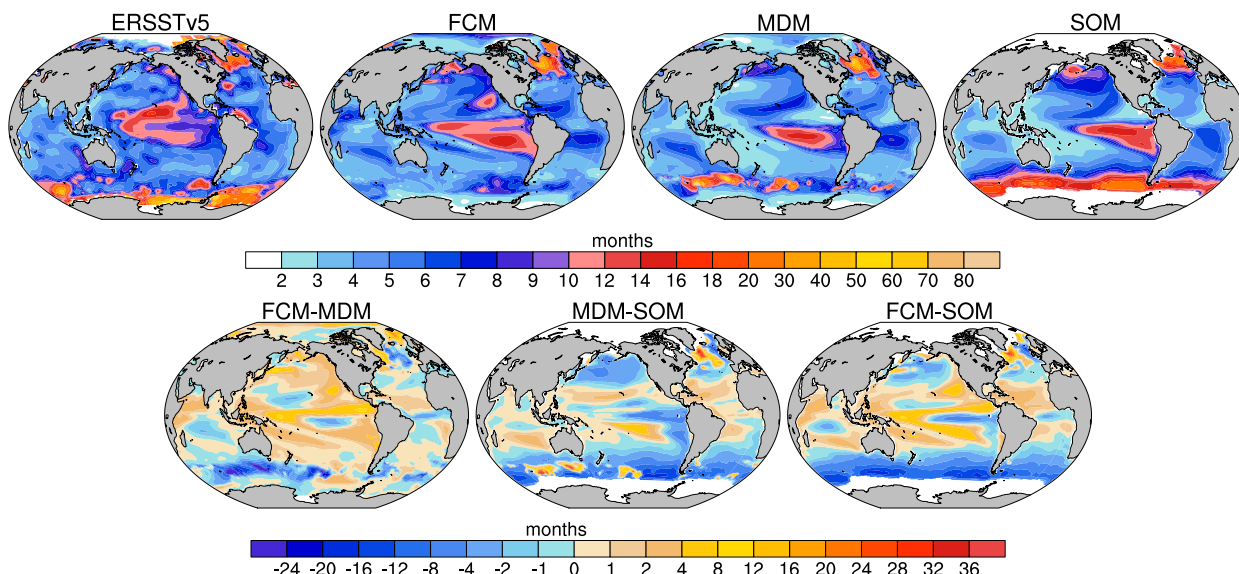
FIG. 7. (top) Persistence in months of anomalous SST in ERSST.v5 and the CESM2 FCM, MDM, and SOM. The persistence time scale is estimated following the DelSole (2001) approach. (bottom) Difference in the persistence time scale between each model version.

longer SOM persistence is due to the lack of a process or processes present in both the MDM and the FCM. We suspect that the lack of ocean damping processes, including vertical mixing, entrainment, and advection by the mean ocean circulation, allows for larger thermodynamically driven SST anomalies and stronger cloud–SST feedbacks (e.g., Fig. 6) in the SOM, leading to higher SST variance with prolonged persistence. At high latitudes, this discrepancy could be due to the lack of wind-driven mixing in the SOM as well as the

differences in the climatological MLD (Fig. 3). Inclusion of τ' dynamics as in the FCM leads to higher SST anomaly variance (Fig. 5) and longer persistence time scales (Fig. 7) in most regions compared to the MDM. For example, longer SST anomaly persistence in the KOE region in the FCM compared to the MDM is consistent with anomalous wind stress–driven processes known to drive SST anomalies on low-frequency time scales through slowly moving off-equatorial oceanic Rossby waves.
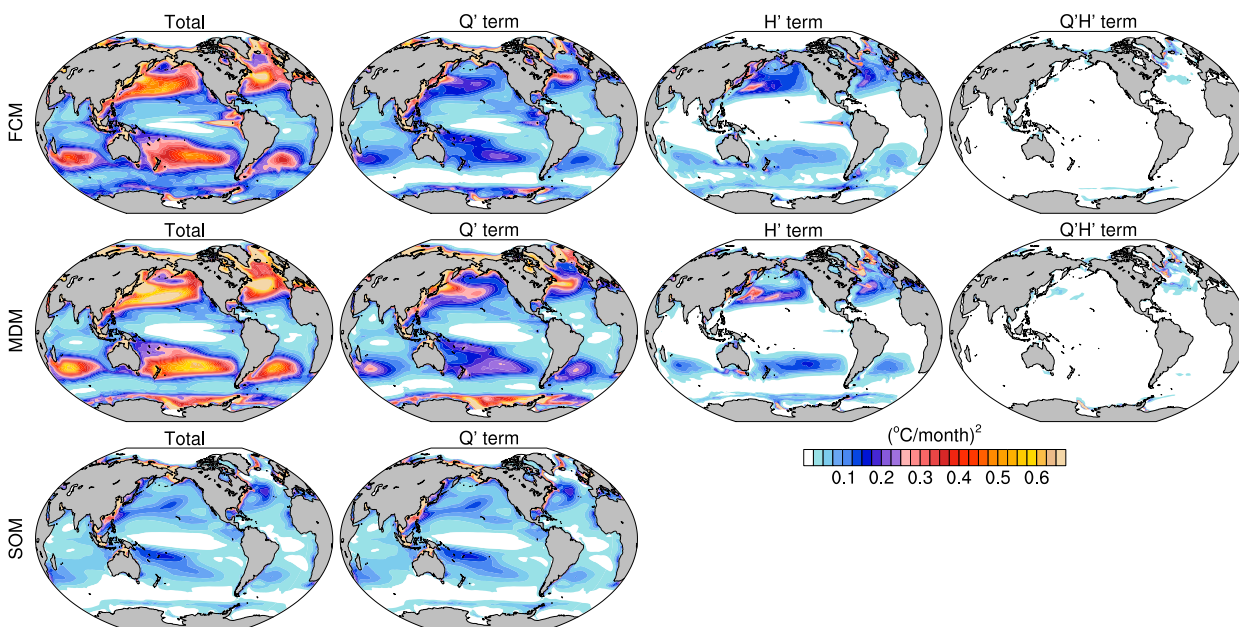
FIG. 8. Variance in (first column) the Q'_{total} term and (from second to fourth columns) the individual Q', H', and $Q'H'$ terms in Eq. (4) for the (top) FCM, (middle) MDM, and (bottom) SOM CESM2 [the units are expressed in $(°C \text{ month}^{-1})^2$].
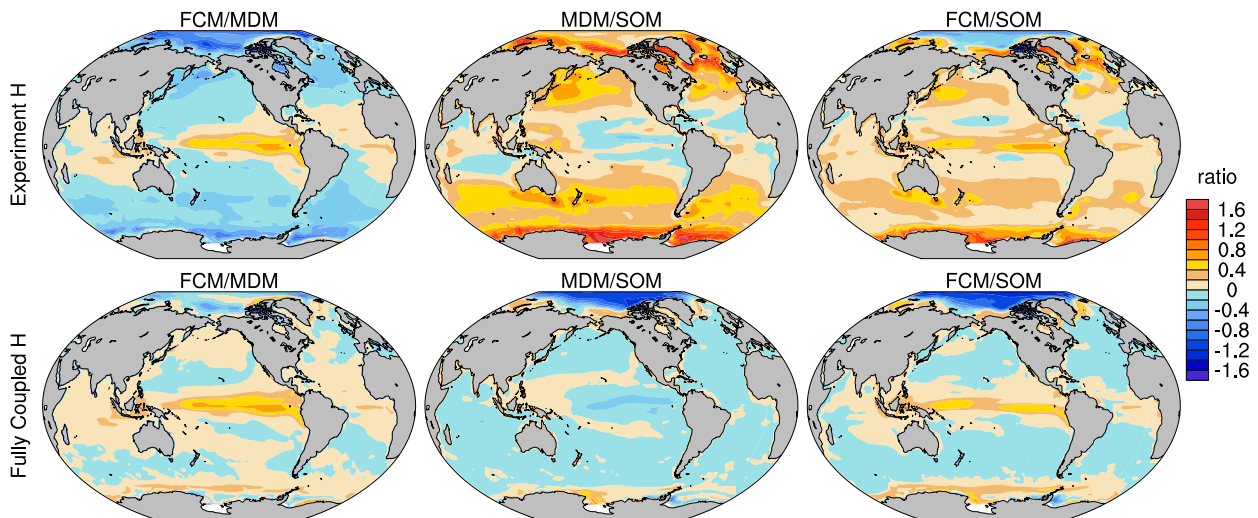
FIG. 9. The common logarithm of the variance ratio of the Q' term for each model pair. (top) The ratio when Q' is computed using the MLD climatology for the respective model. (bottom) Similar ratios except that the monthly MLD climatology from the FCM is used for all models' Q' computation.

The persistence time scale of SST anomalies in the southeast Pacific is markedly large (>12 months) in all models and longer than that in ERSST.v5 (Fig. 7). The presence of these persistent anomalies in all models indicates that thermodynamic coupling is the primary physical mechanism driving the SST changes in this region. Additionally, the southeast Pacific is collocated with the thermally coupled Walker mode (Clement et al. 2011; Zhang et al. 2014), which typically operates on decadal time scales (Okumura 2013) but can be elongated to multidecadal in the presence of positive cloud feedbacks (Bellomo et al. 2014), such as the positive cloud–SST feedback depicted in Fig. 6. These thermodynamically driven persistent SST anomalies appear to overshadow the persistence of canonical ENSO, which shows persistence of 10–12 months only (Fig. 7, FCM panel). In the subtropical northeast Pacific, all models underestimate the SST persistence in ERSST.v5.

e. Impact of climatological MLDs on net surface heat flux forcing

The contribution of anomalous net surface heat flux forcing to SST changes can be determined through Eqs. (5) and (6). The Q'_{total} variance in the SOM is noticeably lower than that in the MDM and FCM (Fig. 8, first column), although determining the origin of this difference is complicated given both Q and H are modified by the presence of a dynamic ocean. The increase in Q'_{total} variance when using a dynamic ocean arises from a combination of 1) inclusion of a varying MLD and 2) dynamic ocean transports that drive SST variability and modulate Q' (Fig. 1). These effects are not easily separable, but the decomposition of Q'_{total} into the three heat flux forcing-related terms in Eq. (6) helps elucidate the relative contributions.

The variance of the Q' term improves understanding of how differences in the mean MLD impact the SST variability

driven by Q' (Fig. 8, second column). Recall that for the SOM, the Q'_{total} term is equivalent to the Q' term, as H in the denominator is constant. The SOM has lower Q' term variance nearly everywhere compared to the MDM and the FCM, especially in the extratropics (Fig. 9, top row, MDM/SOM and FCM/SOM ratios). This finding does not hold when accounting for differences in the MLD climatology: The MDM/SOM and FCM/SOM variance ratios become near zero or negative when substituting the monthly FCM MLD climatology into the denominator of the Q' terms for all models (Fig. 9, bottom row, MDM/SOM and FCM/SOM ratios). These results indicate that the lower variance of the Q' term in the SOM compared to the FCM and the MDM is primarily due to the lack of a seasonally varying MLD climatology. We note that while the variance of Q' itself may vary across models due to differing SST variability that feeds back onto the air–sea heat fluxes, holding the MLD climatology constant (e.g., as in the bottom row of Fig. 9) confirms that the different Q' variability cannot account for the larger overall variance differences in the Q' terms between the models. One exception is in the tropical Pacific, where the role of Q' is to damp SST variability associated with ENSO and Q' is larger in the FCM than the other models (not shown).

We also note that when comparing the FCM and the MDM, the log ratios of the Q' term variance are generally negative (i.e., MDM > FCM) but become more positive when accounting for differences in the monthly MLD climatologies (cf. Fig. 9, top row vs bottom row, FCM/MDM). This result indicates that the MDM overestimates anomalous heat flux–driven SST changes, consistent with expectations from the shallower MLD in the MDM.

Since the MLD in the SOM is constant, the H' and $Q'H'$ terms can only be compared between the MDM and the FCM, although the relative contribution of $Q'H'$ is small. Variability in the H' term (Fig. 8, third column) occurs
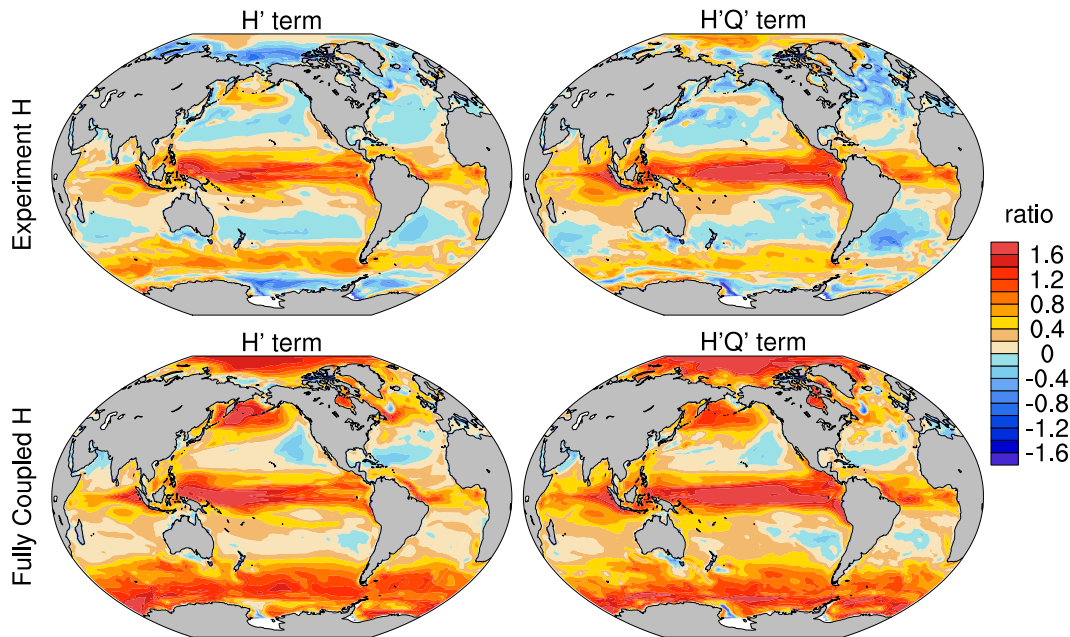
FIG. 10. The common logarithm of the variance ratio (FCM/MDM) of the H' term and $Q'H'$ for the MDM and FCM. (top) The ratio when each term is computed using the MLD climatology for the respective model. (bottom) Similar except that the monthly MLD climatology from the FCM is used for both the FCM and MDM computations.

primarily in the extratropics where wind stress–driven and buoyancy-driven changes in the MLD tend to be largest (e.g., Amaya et al. 2021) (Fig. 8, third column). Seasonally, the largest variability in the H' term occurs in the summer hemisphere (Fig. S9) when the MLD is seasonally shallowest. The FCM also exhibits variability in the H' term in the eastern tropical Pacific related to ENSO, as the MLD is altered via wind-driven upwelling anomalies off the west coast of South America. In both models, variability in the $Q'H'$ term is generally small everywhere except for regions of deep convection (Fig. 8, fourth column), but this is also where the $H'/\overline{H} \ll 1$ assumption breaks down. For both H' and $Q'H'$ terms, the variance ratios become more positive when accounting for differences in the MLD climatology (Fig. 10, compare top and bottom rows). In other words, the shallower climatological MLD in the MDM causes an overestimation in the buoyancy-driven contribution to the variability of the H' and $Q'H'$ terms in the MDM, similar to what was seen with the Q' term comparison. However, we expect the impact of the $Q'H'$ term overestimation in the MDM to be minimal given its smaller magnitude compared to the other terms (Fig. 8). This analysis provides further evidence that the shallower year-round MLD in the MDM leads to larger anomalous heat flux–driven SST variability compared to the FCM. Consequently, when comparing the overall SST variability between the MDM and the FCM, the higher-amplitude heat flux–driven SST variability in the MDM may result in an underestimation of the role of τ' dynamics in driving SST variability.

Finally, we note that the H' and Q' terms in both the FCM and the MDM generally exhibit a positive temporal correlation in the extratropics and eastern tropical Pacific (Fig. S10).

Both the H' and Q' terms exhibit a negative correlation with $Q'H'$ term in the extratropics. So, the $Q'H'$ term which is absent in the SOM generally damps the H'- and Q'-driven extratropical warming or cooling, but its overall contribution to the overall variability is low (Fig. 8). The H' term which is also absent in the SOM has a more pronounced effect on the overall variability and amplifies the warming or cooling tendency driven by Q' term. While, in part, the lower Q'_{total} variability in the SOM is related to the seasonally invariant MLD through the lower Q' term variance, the lack of the H' term also contributes to the overall lower Q'_{total} variability. These results further indicate that while the SOM generally has higher SST variance than the models with more complex oceans, with the exception of regions with large dynamically driven SST variability (i.e., ENSO region, Kuroshio Extension, and Southern Ocean), the higher variability in the SOM is not due to larger heat flux forcing of the SST and rather is most likely due to the lack of ocean damping processes and the seasonally invariant MLD.

5. Summary

In this study, we analyze the SST mean state and variability in three preindustrial versions of CESM2 with varying degrees of ocean complexity. Comparing the SOM, MDM, and FCM versions (see Figs. 1 and 2 for model details) allows for a better characterization of the role of ocean damping, τ' dynamics, and the seasonally varying MLD in setting the SST. We find that τ' dynamics in the FCM act to cool the annual-mean SST compared to the MDM (Fig. 4) through wind stress–driven deepening of the MLD year-round (Fig. 3,

second row) and the associated entrainment of cold water from below, as well as consequently, weaker heating of the SST due to the deeper MLD. These results suggest that the rectification of anomalous wind stress–driven ocean variability onto the mean state can play an important role in setting the annual-mean SST in reality. The strong positive cloud–SST feedback in CESM2 (Fig. 6; Fig. S1) may further amplify the warmer mean SST in the MDM compared to the FCM. The annual-mean SST in the SOM is cooler than the MDM, but for other reasons likely related to the seasonally invariant MLD in the SOM or artificial energy sources and sinks related to the SOM experimental design.

Overall, increasing ocean complexity through the addition of a buoyancy coupled dynamic ocean that includes ocean damping processes (SOM → MDM) and τ' dynamics (MDM → FCM) has competing effects on the overall magnitude of SST variability, as quantified via the anomalous SST variance (Fig. 5). Compared to the SOM, adding a buoyancy coupled dynamic ocean as in the MDM substantially damps SST variability through ocean processes. Compared to the MDM, adding τ' dynamics acts to increase SST variability as in the FCM. Upon adding both sources of ocean complexity (SOM → FCM), the overall role of a dynamic ocean model, as contributing to damping or amplification of SST variability, is regionally dependent. Increased SST variance due to τ' dynamics overcomes ocean damping in the tropical Pacific, Kuroshio Extension, and most of the Southern Ocean in the FCM, resulting in enhanced SST variability in the FCM compared to the SOM. In all other regions in the FCM, interactive ocean damping dominates over τ' dynamics, resulting in reduced SST variability compared to the SOM.

The FCM exhibits longer SST anomaly persistence almost everywhere compared to the MDM (Fig. 7), indicating that τ' dynamics typically act to both enhance the variance (Fig. 5) and elongate the time scales of SST anomalies. While the SOM exhibits higher anomalous SST variance than the MDM everywhere (Fig. 5), adding the effects of a buoyancy coupled dynamic ocean (SOM → MDM) acts to shorten the persistence time scales of SST anomalies across the Southern Ocean, parts of the North Atlantic, and the North Pacific (Fig. 7). We hypothesize that the lack of ocean damping processes in the SOM amplifies the SST variance while prolonging the persistence of the SST anomalies. Similarly, the persistence time scales of SST anomalies in the SOM are longer than that in the FCM in these same regions.

Finally, we decompose the net surface heat flux forcing of the SST into contributions from Q', H', and $Q'H'$ and their total [Eq. (6) and Fig. 8]. We find that the SOM has a smaller amplitude total anomalous heat flux forcing term compared to the FCM and the MDM due to the lack of both a seasonally varying MLD (Fig. 9) and the H' term that amplifies Q' term–driven SST warming and cooling (e.g., Fig. S10). Although the heat flux forcing term has smaller variance in the SOM, the lack of ocean damping processes in the SOM still leads to higher SST variance in the SOM than the FCM and the MDM in most regions. Conversely, we find that the MDM has a larger anomalous heat flux forcing term in the extratropics compared to the FCM (Figs. 9 and 10) due to the

shallower MLD that occurs year-round in the MDM. Overall, the net surface heat flux forcing decomposition suggests that while differences in ocean processes can lead to different Q' variability (Fig. 9, bottom row), the differences in the MLD climatologies between the models are an important factor in leading to differences in the SST variability driven by net surface heat fluxes (Fig. 9, top row).

6. Considerations for model comparisons of SST variability

The CESM2 hierarchy presented here is an important first step in creating a systematic coupled model framework aimed at improving process-based understanding of the ocean's role in climate variability. Based on the many differences in the SST variability considered in this study, we offer factors for consideration when interpreting comparisons across model versions. Here, we present a summary of what is revealed in this study to inform potential users of the CESM2 hierarchy.

Considerations for understanding SST variability in the MDM:

- The MDM mean state SST is warmer than that in the FCM due to the reduced wind stress–driven mixing of the upper ocean and resulting shallower year-round MLD. This ubiquitous warming pattern is different from predecessor versions of CESM2 and may be related to the increase in the positive cloud–SST feedback in CESM2 compared to previous versions.
- SST variability in the MDM is lower amplitude and has shorter persistence time scales compared to the FCM due to the lack of τ' dynamics.
- Despite having lower SST variance than the FCM, the MDM simulates a larger net heat flux forcing term in the anomalous SST tendency equation compared to the FCM due to the shallower year-round seasonally MLD in the MDM. The relatively larger heat flux–driven SST variability in the MDM compared to the FCM may lead to an underestimation of the contribution of τ' dynamics to the overall SST variance when comparing the FCM and the MDM.

Considerations for understanding SST variability in the SOM:

- The SOM mean state SST is generally warmer than that in the FCM and the MDM for reasons most likely related to the SOM experimental design and lack of a seasonally varying MLD.
- The SOM generates a larger SST variance than the FCM and the MDM nearly everywhere due to the lack of a dynamic ocean. Yet, the SOM produces a weaker net surface heat flux forcing term in the anomalous SST tendency equation due to the lack of a variable MLD. Therefore, the SOM's larger SST variance must be due to the lack of ocean damping processes that are present in the dynamic ocean component of CESM2.
- Compared to the FCM and MDM, SST anomalies in the SOM exhibit longer persistence in the Southern Ocean,

North Pacific, tropical Pacific, and parts of the North Atlantic due to the lack of ocean damping processes.

7. Discussion

There are, of course, limitations when using any model, and even the FCM version of CESM2 is limited by horizontal resolution and parameterized processes. Simplified ocean configurations like the SOM and the MDM, despite careful efforts, have mean state biases that can impact the interpretations of results. For example, the MDM uses climatological wind stress forcing on the ocean, and the lack of high-frequency wind variability causes a shoaling of the MLD as investigated in detail in Luongo et al. (2024). We have demonstrated here that the shallower MLD in larger thermodynamically forced SST variability than the FCM, which can cause issues when attempting to quantify how much of the FCM SST variance is thermodynamically versus wind stress forced. Luongo et al. (2024) show that including higher-frequency wind stress forcing in an MDM simulation can reduce SST and MLD biases, although the prescribed wind variability can also drive dynamic ocean changes that then complicate process-based studies. Interestingly, while the SOM has higher SST variance than the models with more complex oceans, the higher variability is not due to larger heat flux forcing of the SST, as the Q'_{total} variance is weakest in the SOM (Fig. 8 left column) but rather is due to the lack of ocean damping processes. Moreover, the seasonally invariant MLD in the SOM leads to weakening of the heat flux forcing of the SST, suggesting that if the SOM included a seasonally varying MLD but still did not include ocean damping processes, the larger SST variance in the SOM compared to the models with more complex oceans may actually be more pronounced. However, in the cases of both the SOM and the MDM, knowledge of limitations of the experimental framework can help those using the simulations for process-based studies better interpret differences across the model hierarchy.

The differences in SST variability across the model hierarchy are also not necessarily governed by local processes. In particular, the presence of canonical ENSO variability in the FCM can enhance SST variability and persistence of anomalies through teleconnection mechanisms. Mean state differences related solely to the lack of ENSO are analyzed in a separate study in which the mechanical decoupling is only applied to the tropical Pacific (Sutton et al. 2024). This study finds that even if ENSO amplitude asymmetry is minimal, asymmetries in the resulting teleconnection patterns can impose a bias on the mean state in the FCM that would be absent in an ENSO-neutral simulation such as when the mechanical decoupling is applied solely to the tropical Pacific.

We last expand upon a few intriguing results from the above analysis. First, the largest SST variance in the SOM (Fig. 5) coincides with where the correlation between SWCF and SST is relatively large and positive in CESM2 (Fig. 6). The MDM shows weaker SST variance in similar regions despite also exhibiting a positive shortwave cloud–SST feedback, suggesting that ocean damping substantially reduces the

variability. In most of these regions, the SOM has higher SST variance than the FCM. This result prompts us to conclude that ocean dynamics overwhelmingly damp any added SST variance driven by τ' dynamics, leading to less variability compared to the SOM in these regions of positive cloud feedback with SST. However, it is possible that a different FCM with a weaker shortwave cloud–SST feedback (see Kim et al. 2022 for CMIP5/6) or weaker ocean damping may exhibit higher SST variability than its companion SOM. The relative contribution of cloud feedbacks, ocean damping, and τ' dynamics is likely, in part, model dependent and could be related to differences in the ocean model, atmosphere model, or air–sea coupling (see also Middlemas et al. 2019).

Second, we note that recent analyses of CESM1 models also show that SST variance in the North Atlantic is larger in the SOM than in the FCM (Murphy et al. 2021). Murphy et al. (2021) hypothesize these differences are related to ocean damping in the FCM. This result is generally consistent with the CESM2 hierarchy analyzed here (Fig. 5; MDM/SOM, FCM/SOM panels). However, we note that the reduction in total variance in the North Atlantic relative to the SOM is larger when comparing the MDM to the SOM, rather than the FCM to the SOM (not shown). These results suggest that deducing the relative role of ocean damping solely from a SOM and FCM comparison may underestimate the extent to which ocean damping reduces SST variance. In other words, given that the FCM also includes τ' dynamics, which act to increase SST variability (Fig. 5, FCM/MDM panel), the role of ocean damping is likely underestimated when comparing the SOM to the FCM. The MDM versus SOM comparison instead shows that damping due to ocean processes may play an even larger role in coupled models than hypothesized in prior studies. Indeed, Zhang (2017) argues that ocean damping, rather than net surface heat flux damping, is the dominant damping mechanism of the North Atlantic SST anomalies, thus demonstrating the importance of including a dynamic ocean model when characterizing temperature variations in the subpolar gyre.

We also note that the persistence time scale of SST anomalies in the North Atlantic varies greatly between the SOM and the models with a dynamic ocean (Fig. 7, bottom row). While including a dynamic ocean enhances the persistence of SST anomalies in a relatively confined region near Greenland, the eastern and southern North Atlantic in the SOM exhibit longer-lasting anomalies compared to the FCM and MDM. Given the substantially different MLD in this region in the SOM compared to the other models, we expect that MLD differences, particularly the lack of a seasonally varying MLD in the SOM (e.g., Liu et al. 2023), are a key contributor to this difference in persistence time scales, but this requires further investigation. Our results, as well as conclusions in Liu et al. (2023), further motivate the need to better understand upper ocean mixing and its impact on SST in the North Atlantic and the ocean in general, as even our observationally based knowledge of these processes remains lacking. Moreover, the development and comparison of the SOM to so-called pencil models that include vertical mixing processes will further improve diagnoses of differences seen in the SOM.

Finally, we acknowledge that this hierarchy does not address issues related to ocean model resolution, which is another way to improve the simulation of ocean complexity in coupled model simulations. While the results obtained from this study generally apply to SST on the large scale, the ocean mesoscale adds another layer of processes that alter SST variability on small spatial and temporal scales (Bryan et al. 2010; Siqueira and Kirtman 2016; Bishop et al. 2017; Small et al. 2019, 2020), which then may influence the large scale.

REFERENCES

Alexander, M. A., and C. Deser, 1995: A mechanism for the recurrence of wintertime midlatitude SST anomalies. *J. Phys. Oceanogr.*, **25**, 122–137, https://doi.org/10.1175/1520-0485(1995)025<0122:AMFTRO>2.0.CO;2.

——, and C. Penland, 1996: Variability in a mixed layer ocean model driven by stochastic atmospheric forcing. *J. Climate*, **9**, 2424–2442, https://doi.org/10.1175/1520-0442(1996)009<2424:VIAMLO>2.0.CO;2.

——, J. D. Scott, and C. Deser, 2000: Processes that influence sea surface temperature and ocean mixed layer depth variability in a coupled model. *J. Geophys. Res.*, **105**, 16 823–16 842, https://doi.org/10.1029/2000JC900074.

Amaya, D. J., 2019: The Pacific meridional mode and ENSO: A review. *Curr. Climate Change Rep.*, **5**, 296–307, https://doi.org/10.1007/s40641-019-00142-x.

——, M. A. Alexander, A. Capotondi, C. Deser, K. B. Karnauskas, A. J. Miller, and N. J. Mantua, 2021: Are long-term changes in mixed layer depth influencing North Pacific marine heatwaves? *Bull. Amer. Meteor. Soc.*, **102**, S59–S66, https://doi.org/10.1175/BAMS-D-20-0144.1.

Barsugli, J. J., and D. S. Battisti, 1998: The basic effects of atmosphere–ocean thermal coupling on midlatitude variability. *J. Atmos. Sci.*, **55**, 477–493, https://doi.org/10.1175/1520-0469(1998)055<0477:TBEOAO>2.0.CO;2.

Battisti, D. S., and A. C. Hirst, 1989: Interannual variability in a tropical atmosphere–ocean model: Influence of the basic state, ocean geometry and nonlinearity. *J. Atmos. Sci.*, **46**, 1687–1712, https://doi.org/10.1175/1520-0469(1989)046<1687:IVIATA>2.0.CO;2.

Bellomo, K., A. Clement, T. Mauritsen, G. Rädel, and B. Stevens, 2014: Simulating the role of subtropical stratocumulus clouds in driving Pacific climate variability. *J. Climate*, **27**, 5119–5131, https://doi.org/10.1175/JCLI-D-13-00548.1.

Bellucci, A., and Coauthors, 2021: Air-sea interaction over the Gulf Stream in an ensemble of HighResMIP present climate simulations. *Climate Dyn.*, **56**, 2093–2111, https://doi.org/10.1007/s00382-020-05573-z.

Bishop, S. P., R. J. Small, F. O. Bryan, and R. A. Tomas, 2017: Scale dependence of midlatitude air–sea interaction. *J. Climate*, **30**, 8207–8221, https://doi.org/10.1175/JCLI-D-17-0159.1.

Bitz, C. M., K. M. Shell, P. R. Gent, D. A. Bailey, G. Danabasoglu, K. C. Armour, M. M. Holland, and J. T. Kiehl, 2012: Climate sensitivity of the Community Climate System Model, version 4. *J. Climate*, **25**, 3053–3070, https://doi.org/10.1175/JCLI-D-11-00290.1.

Bjerknes, J., 1969: Atmospheric teleconnections from the equatorial Pacific. *Mon. Wea. Rev.*, **97**, 163–172, https://doi.org/10.1175/1520-0493(1969)097<0163:ATFTEP>2.3.CO;2.

Bladé, I., 1997: The influence of midlatitude ocean–atmosphere coupling on the low-frequency variability of a GCM. Part I: No tropical SST forcing. *J. Climate*, **10**, 2087–2106, https://doi.org/10.1175/1520-0442(1997)010<2087:TIOMOA>2.0.CO;2.

Bryan, F. O., R. Tomas, J. M. Dennis, D. B. Chelton, N. G. Loeb, and J. L. McClean, 2010: Frontal scale air–sea interaction in high-resolution coupled climate models. *J. Climate*, **23**, 6277–6291, https://doi.org/10.1175/2010JCLI3665.1.

Buckley, M. W., T. DelSole, M. S. Lozier, and L. Li, 2019: Predictability of North Atlantic sea surface temperature and upper-ocean heat content. *J. Climate*, **32**, 3005–3023, https://doi.org/10.1175/JCLI-D-18-0509.1.

Cane, M. A., A. C. Clement, L. N. Murphy, and K. Bellomo, 2017: Low-pass filtering, heat flux, and Atlantic multidecadal variability. *J. Climate*, **30**, 7529–7553, https://doi.org/10.1175/JCLI-D-16-0810.1.

Capotondi, A., and P. D. Sardeshmukh, 2015: Optimal precursors of different types of ENSO events. *Geophys. Res. Lett.*, **42**, 9952–9960, https://doi.org/10.1002/2015GL066171.

——, C. Deser, A. S. Phillips, Y. Okumura, and S. M. Larson, 2020: ENSO and Pacific decadal variability in the Community Earth System Model Version 2. *J. Adv. Model. Earth Syst.*, **12**, e2019MS002022, https://doi.org/10.1029/2019MS002022.

Clement, A., P. DiNezio, and C. Deser, 2011: Rethinking the ocean's role in the Southern Oscillation. *J. Climate*, **24**, 4056–4072, https://doi.org/10.1175/2011JCLI3973.1.

——, K. Bellomo, L. N. Murphy, M. A. Cane, T. Mauritsen, G. Rädel, and B. Stevens, 2015: The Atlantic multidecadal oscillation without a role for ocean circulation. *Science*, **350**, 320–324, https://doi.org/10.1126/science.aab3980.

Danabasoglu, G., and Coauthors, 2020: The Community Earth System Model Version 2 (CESM2). *J. Adv. Model. Earth Syst.*, **12**, e2019MS001916, https://doi.org/10.1029/2019MS001916.

DelSole, T., 2001: Optimally persistent patterns in time-varying fields. *J. Atmos. Sci.*, **58**, 1341–1356, https://doi.org/10.1175/1520-0469(2001)058<1341:OPPITV>2.0.CO;2.

Deser, C., M. A. Alexander, and M. S. Timlin, 1999: Evidence for a wind-driven intensification of the Kuroshio Current extension from the 1970s to the 1980s. *J. Climate*, **12**, 1697–1706, https://doi.org/10.1175/1520-0442(1999)012<1697:EFAWDI>2.0.CO;2.

——, ——, and ——, 2003: Understanding the persistence of sea surface temperature anomalies in midlatitudes. *J. Climate*, **16**, 57–72, https://doi.org/10.1175/1520-0442(2003)016<0057:UTPOSS>2.0.CO;2.

Ding, H., R. J. Greatbatch, W. Park, M. Latif, V. A. Semenov, and X. Sun, 2014: The variability of the East Asian summer monsoon and its relationship to ENSO in a partially coupled climate model. *Climate Dyn.*, **42**, 367–379, https://doi.org/10.1007/s00382-012-1642-3.

——, ——, M. Latif, and W. Park, 2015: The impact of sea surface temperature bias on equatorial Atlantic interannual variability in partially coupled model experiments. *Geophys. Res. Lett.*, **42**, 5540–5546, https://doi.org/10.1002/2015GL064799.

Dong, S., S. T. Gille, and J. Sprintall, 2007: An assessment of the Southern Ocean mixed layer heat budget. *J. Climate*, **20**, 4425–4442, https://doi.org/10.1175/JCLI4259.1.

Eyring, V., S. Bony, G. A. Meehl, C. A. Senior, B. Stevens, R. J. Stouffer, and K. E. Taylor, 2016: Overview of the Coupled Model Intercomparison Project Phase 6 (CMIP6) experimental design and organization. *Geosci. Model Dev.*, **9**, 1937–1958, https://doi.org/10.5194/gmd-9-1937-2016.

Ferreira, D., C. Frankignoul, and J. Marshall, 2001: Coupled ocean–atmosphere dynamics in a simple midlatitude climate model. *J. Climate*, **14**, 3704–3723, https://doi.org/10.1175/1520-0442(2001)014<3704:COADIA>2.0.CO;2.

Frankignoul, C., 1985: Sea surface temperature anomalies, planetary waves, and air-sea feedback in the middle latitudes. *Rev. Geophys.*, **23**, 357–390, https://doi.org/10.1029/RG023i004p00357.

——, and K. Hasselmann, 1977: Stochastic climate models, Part II Application to sea-surface temperature anomalies and thermocline variability. *Tellus*, **29**, 289–305, https://doi.org/10.3402/tellusa.v29i4.11362.

Gozdz, O., M. W. Buckley, and T. DelSole, 2024: The impact of interactive ocean dynamics on Atlantic sea surface temperature variability. *J. Climate*, **37**, 2937–2964, https://doi.org/10.1175/JCLI-D-23-0609.1.

Gu, D., and S. G. H. Philander, 1997: Interdecadal climate fluctuations that depend on exchanges between the tropics and extratropics. *Science*, **275**, 805–807, https://doi.org/10.1126/science.275.5301.805.

Hartmann, D. L., and D. A. Short, 1980: On the use of Earth radiation budget statistics for studies of clouds and climate. *J. Atmos. Sci.*, **37**, 1233–1250, https://doi.org/10.1175/1520-0469(1980)037<1233:OTUOER>2.0.CO;2.

Hasan, M., S. Larson, and K. McMonigal, 2022: Hadley cell edge modulates the role of Ekman heat flux in a future climate.

Geophys. Res. Lett., **49**, e2022GL100401, https://doi.org/10.1029/2022GL100401.

He, C., A. C. Clement, M. A. Cane, L. N. Murphy, J. M. Klavans, and T. M. Fenske, 2022: A North Atlantic warming hole without ocean circulation. *Geophys. Res. Lett.*, **49**, e2022GL100420, https://doi.org/10.1029/2022GL100420.

Huang, B., and Coauthors, 2017: Extended Reconstructed Sea Surface Temperature, version 5 (ERSSTv5): Upgrades, validations, and intercomparisons. *J. Climate*, **30**, 8179–8205, https://doi.org/10.1175/JCLI-D-16-0836.1.

Hunke, E. C., W. H. Lipscomb, A. K. Turner, N. Jeffery, and S. Elliot, 2015: CICE: The Los Alamos Sea Ice Model documentation and software user's manual, version 5.1. Tech. Rep. LA-CC-06-012, 116 pp., https://svn-ccsm-models.cgd.ucar.edu/cesm1/alphas/branches/cesm1_5_alpha04c_timers/components/cice/src/doc/cicedoc.pdf.

Jin, F.-F., 1997: An equatorial ocean recharge paradigm for ENSO. Part I: Conceptual model. *J. Atmos. Sci.*, **54**, 811–829, https://doi.org/10.1175/1520-0469(1997)054<0811:AEORPF>2.0.CO;2.

Joh, Y., and Coauthors, 2022: Seasonal-to-decadal variability and prediction of the Kuroshio Extension in the GFDL coupled ensemble reanalysis and forecasting system. *J. Climate*, **35**, 3515–3535, https://doi.org/10.1175/JCLI-D-21-0471.1.

Kang, S. M., I. M. Held, D. M. W. Frierson, and M. Zhao, 2008: The response of the ITCZ to extratropical thermal forcing: Idealized slab-ocean experiments with a GCM. *J. Climate*, **21**, 3521–3532, https://doi.org/10.1175/2007JCLI2146.1.

Kim, H., S. M. Kang, J. E. Kay, and S.-P. Xie, 2022: Subtropical clouds key to Southern Ocean teleconnections to the tropical Pacific. *Proc. Natl. Acad. Sci. USA*, **119**, e2200514119, https://doi.org/10.1073/pnas.2200514119.

Kwon, Y.-O., and C. Deser, 2007: North Pacific decadal variability in the Community Climate System Model version 2. *J. Climate*, **20**, 2416–2433, https://doi.org/10.1175/JCLI4103.1.

Larson, S. M., and B. P. Kirtman, 2015: Revisiting ENSO coupled instability theory and SST error growth in a fully coupled model. *J. Climate*, **28**, 4724–4742, https://doi.org/10.1175/JCLI-D-14-00731.1.

——, ——, and D. J. Vimont, 2017: A framework to decompose wind-driven biases in climate models applied to CCSM/CESM in the eastern Pacific. *J. Climate*, **30**, 8763–8782, https://doi.org/10.1175/JCLI-D-17-0099.1.

——, K. V. Pegion, and B. P. Kirtman, 2018a: The South Pacific meridional mode as a thermally driven source of ENSO amplitude modulation and uncertainty. *J. Climate*, **31**, 5127–5145, https://doi.org/10.1175/JCLI-D-17-0722.1.

——, D. J. Vimont, A. C. Clement, and B. P. Kirtman, 2018b: How momentum coupling affects SST variance and large-scale Pacific climate variability in CESM. *J. Climate*, **31**, 2927–2944, https://doi.org/10.1175/JCLI-D-17-0645.1.

——, M. W. Buckley, and A. C. Clement, 2020: Extracting the buoyancy-driven Atlantic meridional overturning circulation. *J. Climate*, **33**, 4697–4714, https://doi.org/10.1175/JCLI-D-19-0590.1.

Latif, M., and T. P. Barnett, 1994: Causes of decadal climate variability over the North Pacific and North America. *Science*, **266**, 634–637, https://doi.org/10.1126/science.266.5185.634.

Lau, N.-C., and M. J. Nath, 1996: The role of the "atmospheric bridge" in linking tropical Pacific ENSO events to extratropical SST anomalies. *J. Climate*, **9**, 2036–2057, https://doi.org/10.1175/1520-0442(1996)009<2036:TROTBI>2.0.CO;2.

Lawrence, D. M., and Coauthors, 2019: The Community Land Model version 5: Description of new features, benchmarking, and impact of forcing uncertainty. *J. Adv. Model. Earth Syst.*, **11**, 4245–4287, https://doi.org/10.1029/2018MS001583.

Liu, G., Y.-O. Kwon, C. Frankignoul, and J. Lu, 2023: Understanding the drivers of Atlantic multidecadal variability using a stochastic model hierarchy. *J. Climate*, **36**, 1043–1058, https://doi.org/10.1175/JCLI-D-22-0309.1.

Lübbecke, J. F., B. Rodríguez-Fonseca, I. Richter, M. Martín-Rey, T. Losada, I. Polo, and N. S. Keenlyside, 2018: Equatorial Atlantic variability—Modes, mechanisms, and global teleconnections. *Wiley Interdiscip. Rev.: Climate Change*, **9**, e527, https://doi.org/10.1002/wcc.527.

Luongo, M. T., N. G. Brizuela, I. Eisenman, and S.-P. Xie, 2024: Retaining short-term variability reduces mean state biases in wind stress overriding simulations. *J. Adv. Model. Earth Syst.*, **16**, e2023MS003665, https://doi.org/10.1029/2023MS003665.

McCreary, J. P., Jr., 1983: A model of tropical ocean-atmosphere interaction. *Mon. Wea. Rev.*, **111**, 370–387, https://doi.org/10.1175/1520-0493(1983)111<0370:AMOTOA>2.0.CO;2.

McMonigal, K., and S. M. Larson, 2022: ENSO explains the link between Indian Ocean dipole and meridional ocean heat transport. *Geophys. Res. Lett.*, **49**, e2021GL095796, https://doi.org/10.1029/2021GL095796.

——, S. Larson, S. Hu, and R. Kramer, 2023: Historical changes in wind-driven ocean circulation can accelerate global warming. *Geophys. Res. Lett.*, **50**, e2023GL102846, https://doi.org/10.1029/2023GL102846.

Meccia, V. L., D. Iovino, and A. Bellucci, 2021: North Atlantic gyre circulation in PRIMAVERA models. *Climate Dyn.*, **56**, 4075–4090, https://doi.org/10.1007/s00382-021-05686-z.

Middlemas, E., A. Clement, and B. Medeiros, 2019: Contributions of atmospheric and oceanic feedbacks to subtropical northeastern sea surface temperature variability. *Climate Dyn.*, **53**, 6877–6890, https://doi.org/10.1007/s00382-019-04964-1.

Miller, A. J., D. R. Cayan, and W. B. White, 1998: A westward-intensified decadal change in the North Pacific thermocline and gyre-scale circulation. *J. Climate*, **11**, 3112–3127, https://doi.org/10.1175/1520-0442(1998)011<3112:AWIDCI>2.0.CO;2.

Murphy, L. N., J. M. Klavans, A. C. Clement, and M. A. Cane, 2021: Investigating the roles of external forcing and ocean circulation on the Atlantic multidecadal SST variability in a large ensemble climate model hierarchy. *J. Climate*, **34**, 4835–4849, https://doi.org/10.1175/JCLI-D-20-0167.1.

Newman, M., and Coauthors, 2016: The Pacific decadal oscillation, revisited. *J. Climate*, **29**, 4399–4427, https://doi.org/10.1175/JCLI-D-15-0508.1.

Norris, J. R., and C. B. Leovy, 1994: Interannual variability in stratiform cloudiness and sea surface temperature. *J. Climate*, **7**, 1915–1925, https://doi.org/10.1175/1520-0442(1994)007<1915:IVISCA>2.0.CO;2.

Okumura, Y. M., 2013: Origins of tropical Pacific decadal variability: Role of stochastic atmospheric forcing from the South Pacific. *J. Climate*, **26**, 9791–9796, https://doi.org/10.1175/JCLI-D-13-00448.1.

Putrasahan, D. A., O. Gutjahr, H. Haak, J. H. Jungclaus, K. Lohmann, M. J. Roberts, and J.-S. von Storch, 2021: Effect of resolving ocean eddies on the transient response of global mean surface temperature to abrupt 4xCO$_2$ forcing. *Geophys. Res. Lett.*, **48**, e2020GL092049, https://doi.org/10.1029/2020GL092049.

Qiu, B., 2003: Kuroshio extension variability and forcing of the Pacific decadal oscillations: Responses and potential feedback.

J. Phys. Oceanogr., **33**, 2465–2482, https://doi.org/10.1175/1520-0485(2003)033<2465:KEVAFO>2.0.CO;2.

Rädel, G., T. Mauritsen, B. Stevens, D. Dommenget, D. Matei, K. Bellomo, and A. Clement, 2016: Amplification of El Niño by cloud longwave coupling to atmospheric circulation. *Nat. Geosci.*, **9**, 106–110, https://doi.org/10.1038/ngeo2630.

Rintoul, S. R., and M. H. England, 2002: Ekman transport dominates local air–sea fluxes in driving variability of subantarctic mode water. *J. Phys. Oceanogr.*, **32**, 1308–1321, https://doi.org/10.1175/1520-0485(2002)032<1308:ETDLAS>2.0.CO;2.

Saravanan, R., and P. Chang, 1999: Oceanic mixed layer feedback and tropical Atlantic variability. *Geophys. Res. Lett.*, **26**, 3629–3632, https://doi.org/10.1029/1999GL010468.

Schneider, N., and A. J. Miller, 2001: Predicting western North Pacific Ocean climate. *J. Climate*, **14**, 3997–4002, https://doi.org/10.1175/1520-0442(2001)014<3997:PWNPOC>2.0.CO;2.

——, ——, and D. W. Pierce, 2002: Anatomy of North Pacific decadal variability. *J. Climate*, **15**, 586–605, https://doi.org/10.1175/1520-0442(2002)015<0586:AONPDV>2.0.CO;2.

Seager, R., Y. Kushnir, M. Visbeck, N. Naik, J. Miller, G. Krahmann, and H. Cullen, 2000: Causes of Atlantic Ocean climate variability between 1958 and 1998. *J. Climate*, **13**, 2845–2862, https://doi.org/10.1175/1520-0442(2000)013<2845:COAOCV>2.0.CO;2.

——, ——, N. H. Naik, M. A. Cane, and J. Miller, 2001: Wind-driven shifts in the latitude of the Kuroshio–Oyashio Extension and generation of SST anomalies on decadal timescales. *J. Climate*, **14**, 4249–4265, https://doi.org/10.1175/1520-0442(2001)014<4249:WDSITL>2.0.CO;2.

Siqueira, L., and B. P. Kirtman, 2016: Atlantic near-term climate variability and the role of a resolved Gulf Stream. *Geophys. Res. Lett.*, **43**, 3964–3972, https://doi.org/10.1002/2016GL068694.

Small, R. J., F. O. Bryan, S. P. Bishop, and R. A. Tomas, 2019: Air–sea turbulent heat fluxes in climate models and observational analyses: What drives their variability? *J. Climate*, **32**, 2397–2421, https://doi.org/10.1175/JCLI-D-18-0576.1.

——, ——, ——, S. Larson, and R. A. Tomas, 2020: What drives upper-ocean temperature variability in coupled climate models and observations? *J. Climate*, **33**, 577–596, https://doi.org/10.1175/JCLI-D-19-0295.1.

Smith, D. M., and Coauthors, 2019: Robust skill of decadal climate predictions. *npj Climate Atmos. Sci.*, **2**, 13, https://doi.org/10.1038/s41612-019-0071-y.

Smith, R., and Coauthors, 2010: The Parallel Ocean Program (POP) reference manual. Tech. Doc. LAUR-10-01853, 141 pp., https://www2.cesm.ucar.edu/models/cesm1.0/pop2/doc/sci/POPRefManual.pdf.

Stuecker, M. F., A. Timmermann, F.-F. Jin, Y. Chikamoto, W. Zhang, A. T. Wittenberg, E. Widiasih, and S. Zhao, 2017: Revisiting ENSO/Indian Ocean dipole phase relationships. *Geophys. Res. Lett.*, **44**, 2481–2492, https://doi.org/10.1002/2016GL072308.

Suarez, M. J., and P. S. Schopf, 1988: A delayed action oscillator for ENSO. *J. Atmos. Sci.*, **45**, 3283–3287, https://doi.org/10.1175/1520-0469(1988)045<3283:ADAOFE>2.0.CO;2.

Sutton, M., S. M. Larson, and E. Becker, 2024: New insights on ENSO teleconnection asymmetry and ENSO forced atmospheric circulation variability over North America. *Climate Dyn.*, **62**, 3189–3206, https://doi.org/10.1007/s00382-023-07058-1.

Sutton, R., and P.-P. Mathieu, 2002: Response of the atmosphere–ocean mixed-layer system to anomalous ocean heat-flux

convergence. *Quart. J. Roy. Meteor. Soc.*, **128**, 1259–1275, https://doi.org/10.1256/003590002320373283.

Takahashi, N., K. J. Richards, N. Schneider, H. Annamalai, W.-C. Hsu, and M. Nonaka, 2021: Formation mechanism of warm SST anomalies in 2010s around Hawaii. *J. Geophys. Res. Oceans*, **126**, e2021JC017763, https://doi.org/10.1029/2021JC017763.

Tsartsali, E. E., and Coauthors, 2022: Impact of resolution on the atmosphere–ocean coupling along the Gulf Stream in global high resolution models. *Climate Dyn.*, **58**, 3317–3333, https://doi.org/10.1007/s00382-021-06098-9.

Xie, S.-P., and S. G. H. Philander, 1994: A coupled ocean-atmosphere model of relevance to the ITCZ in the eastern Pacific. *Tellus*, **46A**, 340–350, https://doi.org/10.3402/tellusa.v46i4.15484.

Yamamoto, A., H. Tatebe, and M. Nonaka, 2020: On the emergence of the Atlantic multidecadal SST signal: A key role of the mixed layer depth variability driven by North Atlantic Oscillation. *J. Climate*, **33**, 3511–3531, https://doi.org/10.1175/JCLI-D-19-0283.1.

Yang, Y., S.-P. Xie, L. Wu, Y. Kosaka, N.-C. Lau, and G. A. Vecchi, 2015: Seasonality and predictability of the Indian Ocean dipole mode: ENSO forcing and internal variability. *J. Climate*, **28**, 8021–8036, https://doi.org/10.1175/JCLI-D-15-0078.1.

Yeager, S., 2020: The abyssal origins of North Atlantic decadal predictability. *Climate Dyn.*, **55**, 2253–2271, https://doi.org/10.1007/s00382-020-05382-4.

Yulaeva, E., N. Schneider, D. W. Pierce, and T. P. Barnett, 2001: Modeling of North Pacific climate variability forced by oceanic heat flux anomalies. *J. Climate*, **14**, 4027–4046, https://doi.org/10.1175/1520-0442(2001)014<4027:MONPCV>2.0.CO;2.

Zebiak, S. E., 1993: Air–sea interaction in the equatorial Atlantic region. *J. Climate*, **6**, 1567–1586, https://doi.org/10.1175/1520-0442(1993)006<1567:AIITEA>2.0.CO;2.

——, and M. A. Cane, 1987: A model El Niño–Southern Oscillation. *Mon. Wea. Rev.*, **115**, 2262–2278, https://doi.org/10.1175/1520-0493(1987)115<2262:AMENO>2.0.CO;2.

Zhang, H., A. Clement, and P. Di Nezio, 2014: The South Pacific meridional mode: A mechanism for ENSO-like variability. *J. Climate*, **27**, 769–783, https://doi.org/10.1175/JCLI-D-13-00082.1.

Zhang, R., 2017: On the persistence and coherence of subpolar sea surface temperature and salinity anomalies associated with the Atlantic multidecadal variability. *Geophys. Res. Lett.*, **44**, 7865–7875, https://doi.org/10.1002/2017GL074342.

——, R. Sutton, G. Danabasoglu, T. L. Delworth, W. M. Kim, J. Robson, and S. G. Yeager, 2016: Comment on "The Atlantic multidecadal oscillation without a role for ocean circulation". *Science*, **352**, 1527, https://doi.org/10.1126/science.aaf1660.

——, ——, ——, Y.-O. Kwon, R. Marsh, S. G. Yeager, D. E. Amrhein, and C. M. Little, 2019: A review of the role of the Atlantic meridional overturning circulation in Atlantic multidecadal variability and associated climate impacts. *Rev. Geophys.*, **57**, 316–375, https://doi.org/10.1029/2019RG000644.

Zhang, Y., and Coauthors, 2021: Pacific meridional modes without equatorial Pacific influence. *J. Climate*, **34**, 5285–5301, https://doi.org/10.1175/JCLI-D-20-0573.1.